REPUBLIC OF AZERBAIJAN

On the rights of the manuscript

ABSTRACT

of the dissertation for the degree of Doctor of Science

APPLICATION OF DENSITY FUNCTIONAL THEORY IN SYNTHESIS OF VARIOUS HETEROCYCLIC COMPOUNDS, POLY-*p*-PHENYLENEDIAMINE AND SURFACTANTS

Specialty: 2314.01 – Petroleum Chemistry

Field of science: Chemistry

Applicant: Yusif Afraddin Abdullayev

BAKU-2023

The work was performed at the Republic of Azerbaijan Ministry of Education and Sciences, Institute of Petrochemical Processes, named after Yusif Mammadaliyev at the "Corrosion inhibitors and corrosion materials" laboratory № 24

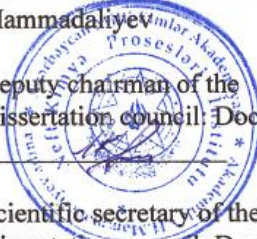**Scientific consultant:** Doctor of Chemical Sciences, Academic,
Vagif Maharram Abbasov

Official opponents: Doctor of Chemical Sciences, Academic,
Ajdar Akbar Majidov

Doctor of Chemical Sciences, professor,
Akbar Ali Agayev

Doctor of Chemical Sciences, professor,
Namig Gurbat Shikhaliyev

Doctor of Chemical Sciences, professor,
Manzar Nezammeddin Amiraslanova

Dissertation council ED 1.16 of Supreme Attestation Commission under the President of the Republic of Azerbaijan operating at Institute of Petrochemical Processes, named after Yusif Mammadaliyev

Deputy chairman of the
Dissertation council: Doctor of Chemical Sciences, prof,
Minavar Jafar Ibrahimova

Scientific secretary of the
Dissertation council: Doctor of Chemical Sciences, Assoc. prof.,
Lala Mahammad Afandiyeva

Chairman of the
scientific seminar: Doctor of Chemical Sciences, Assoc. prof
Fuzuli Akbar Nasirov

2

INTRODUCTION

The relevance of the topic. The organic synthesis current contribution to pharmaceutical, closing, food, and military industries reveals its intense utilization in the future. To enhance the efficiency of synthetic processes, simulation of the organic reaction with computational technics has been quite widespread in the last decade. Especially, using computer clusters prevent time consumption and is economically viable. Parallel processors are utilized in clusters to support many users and carry out calculations in a short time, which takes more time (days, months) if a calculation is conducted on a PC. Computer clusters are being used in weather modeling, computational fluid dynamics, aerodynamics, automobile and aircraft crash simulations, nuclear simulations, image processing, data mining, and life sciences. In organic synthesis, for synthesizing a target molecule, we need to conduct an experiment or sequence of experiments. It may take a couple of days, and separation and purification are required after finishing the experiments. Also, we need to consider the consumption of solvents, which are toxic in most cases, and exposure to the human body during separation or purification, threatening human health. Computational chemistry offers to calculate Gibbs free energies of each component, including substrates, intermediates, transition states, and products, to design potential energy surface (PES) diagrams[1]. According to the PES diagrams, computational chemists could make an idea about the feasibility of a reaction and pass information to experimental chemists. In this manner, only possible reactions can be examined in a lab, preventing extra materials and time consumption. Articles are highly appreciated, and acceptance will be easy in prestigious high-impact journals if, besides experimental work, theoretical calculations are given to support and confirm an experiment. The recent development of high-performance computer clusters supports scientific calculation.

_____
1. L.-P. Xu, N. Li, D.G. Musaev, Mechanistic Details of the Pd-catalyzed and MPAA Ligand-Enabled β-C(sp3)-H Acetoxylation of Free Carboxylic Acid, Chemistry – An Asian Journal, 18 (2023) e202201145.

Computational departments exist in most of the world's well-known universities and industrial institutions to calculate or simulate reactions and processes. As a result of calculation, it would be possible to forecast processes without doing practical work.

The work objective and subject. The research's main objective is to apply DFT calculations to strategic synthesis, e.g., biofuel precursors, pharmacophores, lubricants, surfactants, and carbon dioxide conversion. Utilizing DFT calculations to determine the role of ionic liquids on the aforementioned syntheses. Application of DFT in macromolecular chemistry such as poly-p-phenylenediamine and gemini surfactants synthesis and structural analysis. Identification of the function of initiator and water on the free-radical chain reaction. Optimization of the minimum energy conformers of the gemini surfactant molecules. According to the position of a surfactant head and tail groups, formation Gibbs energy calculations and matching the obtained energies. Application of ionic liquid to the synthesis of cyanuric acid and theoretical studies on the reaction mechanism. Calculation of various substrate and carbon dioxide binding activation energies for the synthesis of heterocyclic organic compounds. Generating a map for experimentalists based on the calculated carbon dioxide binding activation energies.

The purpose of the work is to calculate plausible mechanisms for important syntheses, such as the production of biofuel precursors, pharmaceuticals, and lubricants. Computational identification of ionic liquids' role in the synthesis of multi-substituted imidazole, cyanuric acid, 5-hydroxymethylfurfural, and carbon dioxide conversion to heterocyclic carbonyl derivatives. A computational approach to the free-radical polymerization of p-phenylenediamine to poly-p-phenylenediamine and surfactant synthesis and the macromolecular surfactant molecule optimizations were also considered in this work. Based on the first-principal calculations, generating potential energy surface (PES) profiles, which can be used for kinetic studies. According to PES and kinetic studies, the best reaction route can be determined. Monitoring homogeneous catalysts on the same reaction and determining the efficient one.

Research methods. The theoretical part of the work was

conducted using Gaussian 16 program package. The software uses quantum mechanics to calculate a molecule's vibrational frequencies and total energies in various chemical environments, i.e., gas phase and any solvent of interest. Intrinsic reaction coordinate search (IRC) was used to connect transition states to the related intermediates in a potential energy surface. GaussView 6 software was used in the visualization of the gaussian outputs. Structure elucidations were conducted with NMR, GC-MS, IR, and X-ray crystallography. The synthesized compounds were purified with recrystallization, flash, and column chromatographyc methods. The conducted reactions were monitored with TLC (thin layer chromatography) and GC-MS to see a substrate conversion to a product.

Main points/clauses to defense. Pyrrole-based fused triazepine derivatives were synthesized, and the structure of the synthesized compounds was identified with spectroscopic methods. The related reactions were calculated with DFT to determine the cyclization mechanism.

One pot four components maltisubstituted imizole synthesis with low-cost ionic liquid $[(C_2H_5)_2NH_2][HSO_4]$ as a catalyst (30 mol %) was conducted in a short period of time (20 min.) with quantitative yield (98 %). The catalyst's superior effects (better than metal catalysts) inspired us to conduct mechanistic DFT studies on the reaction. Theoretical studies revealed that the ionic liquid cation and anion components dual catalytic performance accelerated the reaction event better than the previously used indium-based catalyst.

Ionic liquid mediated $[(C_2H_5)_2NH_2][HSO_4]$ tetrasubstituted imidazole and pyrazine synthesis from substrates (benzil and benzylamine) were studied experimentally (in solvent- and metal-free conditions) and computationally. DFT calculations identified that the ring closure is possible via $C(sp^3)$-H activation. The reaction conditions were optimized based on various reaction parameters (time, catalyst loading, temperature, and solvents). It was determined that the reaction could be tuned toward pyrazine synthesis.

One-pot four-component polycyclic imidazole synthesis was conducted with the support of pyperazinium based ionic liquid.

Because of the azo-group containing aromatic scaffold, the synthesized compounds possess fluorescent properties. The ionic liquid role on the cyclization was identified with DFT calculations. TD-DFT was applied to calculate theoretical HOMO-LUMO energy gaps. Quantum yield calculations showed that the synthesized compounds could be used as a substitute of currently used commercially available materials in optoelectronic devices.

Multisubstituted triazinane-2-thione was synthesized from one-pot three-component cyclocondensation of thiourea, ammonia, and benzaldehyde using acetic acid halogenated derivatives. The reaction mechanism was calculated in the presence of acetic acid and its trichloro, tribromo, and trifluoro versions. DFT studies showed that the strong acidity of the catalyst is not a driving force for the reaction. Namely, trichloro acetic acid is a better catalyst than trifluoro acetic acid for the model reaction.

The double bond (C=C) defunctionalization is important because of its versatile application in the industry. The C=C double bonds of vegetable oil were defunctionalized with various peroxy-acids, then subsequent aminolysis resulted in lubricant formation. DFT studies identified the suitable peroxy acid for the process. Theoretical calculations also determined that the $FeCl_2$ catalyst is the best option for the epoxy ring opening.

The conversion of glucose to 5-hydroxymethylfurfural was studied in the presence of N,N-diethyl-1,4-phenylenediamine hydrogen sulfate ionic liquid. Optimizing reaction parameters (catalyst screening, temperature, time, catalyst loading, and solvents) afforded 94 % 5-HMF yield at 160 ºC. The catalyst unique performance was evaluated with DFT calculations.

Computational mechanistic studies were conducted on $K_2S_2O_8$ initiated p-phenylenediamine polymerization taking into account sulfate free-radical (considered to form persulfate decomposition), persulfate anion, and $K_2S_2O_8$ cluster. Computations showed that the $K_2S_2O_8$ cluster is better than other tested species, which results in the dimerization pathway via shallow energy barriers. The potassium

effect was noticed as crucial in decreasing activation energies.

Ionic liquid $[(CH_3)_2NH_2][HSO_4]$ mediated conversion of urea to cyanuric acid was studied experimentally and computationally. Several reaction routes were calculated for cyanuric acid formation. Matching IL-free and IL-incorporated urea trimerization routes showed that applied ionic liquid considerably lowers the trimerization energy barriers. Further investigation proposed that urea decomposition to isocyanic acid then its trimerization to cyanuric acid owns more thermodynamic driving force, which proposed that urea trimerization goes through isocyanic acid. Our computational investigation is in good agreement with previous experimental studies that reported isocyanic acid detection upon heating urea.

Precious metal-catalyzed carbon dioxide conversion reactions to five-membered heterocyclic organic compounds inspired us to test the same reactions with $[(C_2H_5)_2NH_2][HSO_4]$ ionic liquid computationally. Various substrates were taken for the computational mechanistic studies and it was identified that ethylene diamine utilization lowers carbon dioxide binding and ring closure activation energies. Testing several substrates and ionic liquid modifications versus the aforementioned activation energies proposed a map to experimentalists related to carbon dioxide conversion scope.

Propylene oxide ring opening with long chain amines (C_{12}-NH_2) and further coupling of the products with 1,3-dibromopropane to form gemini surfactants were studied computationally. The tail groups orientations and formation Gibbs energy correlations in tertiary and quaternary surfactants were identified.

The novelty of the work. For the first time, computational mechanistic studies were applied to identify the formation mechanism of fused pyrrole-based triazepine derivatives. It was determined that the propargyl group that binds to pyrrole is tautomerize to the allyl group, which has a crucial role in the cyclization to form fused pyrrolo-triazepine derivatives.

As an alternative to homogeneous transition metal catalysis, for the first time the function of diethylammonium hydrosulfate ionic liquid (IL) application on the one-pot four-component cyclization to

polycyclic imidazole derivatives was determined by the theoretical studies. The reaction profile was calculated three times: in the solvent-free, IL-solvation, and IL-catalytic conditions. The studies showed that the IL-catalytic condition energy barriers are dramatically smaller compared to the other two cases.

Based on the experimental observation, it was determined that in a short time (20 min) a ≥90 % reaction yield was achieved. A similar reaction was conducted previously with transition and precious metal catalysts (e.g., the reaction was carried out with indium chloride in 6 h with an 84 % yield). The reason behind the huge difference in the reaction time and yield was scrutinized with the DFT studies, which is associated with the IL cation and anion part dual catalytic effects on the reaction.

Metal and solvent-free synthesis of tetrasubstituted imidazole and tetraphenylpyrazine from benzil and benzyl amine was studied experimentally and computationally. This reaction was carried out previously (D. K. Maiti et. al., 2014 *Chem. Commun.* /C. Mukhopadhyay et. al., 2015 *Eur. J. Org. Chem.*) with metal (Ni and Ag) based catalysts in 10-12 hours in the presence of various solvents at 80ºC and 110ºC. The reaction condition was fundamentally altered in order to make the reaction "greener" and energy efficient. The mentioned metal catalysts from the literatures were substituted with metal-free Brønsted acidic ionic liquids, time was shortened to 1 hour, solvent was abstracted, and temperature was stabilized at 90ºC. Tetrasubstituted imidazole was obtained in 79% yield, and tetraphenylpyrazine (19% yield) was recovered as a byproduct. The impact of five variables has been investigated in relation to the product yields: type of ionic liquids, reaction temperature, reaction time, various polar/nonpolar solvents, and catalyst loading. Optimizations show that the tetraphenylpyrazine yield can be increased to 52%. This product was synthesized (Lochbrunner et al. Tetrahedron 2015) via the Suzukie-Miyaura reaction in two steps in 18 hours: Preparation of tetrachloropyrazine from piperazine-2,5-dione and toxic chemicals (PCl_5/$POCl_3$), followed by arylation of the tetrachloropyrazine with expensive palladium catalysts/ligands and phenylboronic acid. The possibility of tetraphenylpyrazine synthesis via simple Brønsted acidic

ionic liquids in mild condition and in very short time (1 h) was demonstrated. Moreover, the whole cycle for imidazole ring formation mechanism via condensation to diimine, and further $C(sp^3)$–H activated cyclization stages was computed. Crucial intermediates and transition state that lead to pyrazine ring formation were determined. To the best of our knowledge, metal and iodine-free Brønsted acidic ionic liquids were utilized for the first time in $C(sp^3)$–H activation which is currently carried out with expensive transition metal catalysts. Our study offers new insight to Brønsted acidic ILs catalyzed $C(sp^3)$-H bond functionalization reactions.

Polycyclic azo-group containing imidazole derivatives with one-pot four component fusion reaction using 1,4-dimethylpyperazinium dihydrosulfate ($[Me_2pi][HSO_4]_2$) ionic liquid (IL) catalyst (3 mol%) were synthesized. Unlike previous studies, weak basic ((4-(phenyldiazenyl)phenyl)methanamine) aromatic amine was activated using low-cost IL. The catalytic amount of the IL is acting as a superior catalyst than precious metal catalysts previously utilized for the similar one-pot fusion reactions. The computational conformational studies demonstrated that the trans conformer of the IL catalyst is a better catalyst because of the available acidic protons. Important transition states for the rate-limiting step ($\Delta G\ddagger$=26.56 kcal/mol), the five-membered imidazole ring formation ($\Delta G\ddagger$=6.9 kcal/mol), and the C(sp3)-H ($\Delta G\ddagger$=2.06 kcal/mol) activation were optimized. The product fluorescence properties are studied computationally (HOMO and LUMO energy gap=1.59 eV) and experimentally. Acetic acid (AA) and its halogenated derivatives are frequently used as organocatalyst in synthesis of value-added organic compounds. The literature often states that trifluoroacetic acid (TFA) is better among other halogenated AA derivatives as an organocatalyst in synthesis because of its high acidity. There is a few experimental works can be found with the utilization of AA, TFA, and trichloroacetic acid (TCA) as a catalyst on the same reaction. To the best of our knowledge, no theoretical research can be found in the literature related to a deep combined study of AA and its derivatives' catalytic effects on a certain reaction. So, we turn to computation for studying the catalytic effects of AA, TFA, and TCA on a one-pot

multi-component synthesis. We chose (4S,6S)-4,6-diphenyl-1,3,5-triazinane-2-thione (anti-carcinogenic, strong biological activities) formation from thiourea, ammonia, and benzaldehyde as a model reaction. We try to find an answer to the question: Does strong acidity determine better catalytic performance? Plausible mechanisms were determined by first-principles quantum chemical calculations for AA, TFA, and TCA-catalyzed one-pot three-component cyclocondensatin to triazinane-2-thione. We found that TCA is a better catalyst for the model reaction despite its weak acidity than TFA based on the energy span calculations. The trans conformer of triazinane-2-thione is obtained from the final ring closure transition state. Our calculations are in good agreement with the experimental observation showing the trans conformer ((4S,6S)-4,6-diphenyl-1,3,5-triazinane-2-thione) is stable in the water medium (B. Kaboudin, T. Ghasemi and T. Yokomatsu, *Synthesis*, 2009, 3089-3093). The reaction was calculated to be 33.4 kcal/mol endergonic, and experimentally applied temperature (313K) was the satisfactory driving force for the product (85%) formation. Despite the TFA strong acidity, TCA was obtained as an efficient catalyst for the reaction. We applied the energy span model to compute catalytic efficiencies. The energy span model displayed TCA as a relatively better catalyst for the model reaction. In the studied case, acidity is, therefore, not the main predictor for an indicator for catalytic activity selection. The carbon-carbon double bond defunctionalization is very important in the industry. It converted sustainable sources (vegetable oils) to fuel and lubricant precursors. The lack of computational studies and the industrial importance of the reaction inspired us to perform broad studies for the C=C bond epoxidation and the epoxide ring-opening. The mechanistic studies were carried out for the C=C bond epoxidation via computing experimentally tested oxidizing agents. Based on the energy barriers, we defined performic acid (PF) as the best option relative to the other tested two oxidizing agents (hydrogen peroxide (HP) and peracetic acid (PA)). It is often stated in the literature that $ZnCl_2$ catalyzes the epoxide ring opening efficiently. However, to the best of our knowledge, no detailed computational mechanistic studies for the Lewis acidic catalyzed epoxide-ring opening reaction have been

reported. In our research, we aim to compare $ZnCl_2$ and other low-cost transition metal chlorides ($FeCl_2$ and $NiCl_2$) catalytic efficiencies. Instead of the energy barrier for the rate-determining step, we use the energetic span model and theoretical TOF values to evaluate the catalytic cycles for the Lewis acidic catalysts mentioned above. We found that $FeCl_2$-mediated ring-opening is the most efficient catalytic cycle. Our study offers new theoretical insight to experimentalists about the utilization of a low-cost substitute of $ZnCl_2$. The findings are likely to apply to a large variety of other reactions as well. Glucose dehydration to 5-hydroxymethylfurfural (5-HMF) via a low-cost and easily accessible Brønsted acidic ionic liquid (IL, [DPhDA]HSO$_4$) catalyst because of 5-HMF importance as carbon-natural building blocks for the preparation of the versatile chemicals, i.e., fuel precursors, the monomer for the construction of important polymers. A huge number of works reported with Lewis acidic metal catalysis or mixed with IL co-catalysts (or as a solvent), which are not environmentally benign. Only a few studies were conducted with solely IL catalysts: 1-hydroxyethyl-3-methylimidazolium tetrafluoroborate was taken as a catalyst for the conversion of glucose and fructose to 5-HMF without using any Lewis acidic co-catalysts in the presence of DMSO with 67% yield (*Bioresource Technology* **2012,** *121*, 462-466). Metal functionalized IL (1-sulfonic acid-3-methyl imidazolium tetrachloroferrate) was utilized for the same purpose, which yielded lower 5-HMF (18%) and moderate levulinic acid (LA) (68%) from glucose conversion in harsh condition (*Journal of Molecular Catalysis A: Chemical* **2015,** *407*, 113-121). Polyethylene supported IL was applied as a catalyst for fructose dehydration to 5-HMF with 86% yield (*Green Chemistry* **2013,** *15* (12), 3438-3445). As seen from the above literature studies, usage of IL as a catalyst for the 5-HMF production requires improvements for the industrial-scale application. Unlike past research, the proposed IL catalyst is superior and untraditional in terms of 5-HMF selectivity and yield. We achieved nearly a quantitative 5-HMF yield (**<u>94% with 30 mol% in the presence of DMSO at 160ºC</u>**), which can drive scientists' attention who are working on biomass processing. The computational study of the potassium persulfate-initiated polymerization mechanism

of p-phenylenediamine (p-PDA) is crucial to understanding the synthesized polymer scope. The monomer (PDA) is a precursor to aramid plastics and fibers and has extensive applications in electronic devices and the arms industry. p-PDA dimerization step was considered for computation to understand the polymerization pattern. The polymer chain elongation mechanism was proposed based on the replicated free-radical formation (monomer)→ dimerization → ammonia extrusion → free-radical formation (dimer). Since aqueous media was used experimentally, potassium persulfate dissociation was considered, and the steps mentioned above were calculated trice: sulfate free-radical (SFR), persulfate anion (PA), and potassium persulfate (PP) cluster-mediated routes. Because of the lowest formation Gibbs energies of TSs and intermediates, the PP route was studied in detail. The barrierless conversion of p-PDA to free-radical promotes dimerization through the 11.6 kcal/mol energy barrier. Further ammonia extrusion step leads to dimer formation via 6.7 kcal/mol energy. Cyanuric acid is an essential commodity with frequent utilization in the industry as a precursor for the production of chlorine stabilizers, i.e., trichloroisocyanuric acid and sodium dichloroisocyanurate. Because of the growing demand for the noticed products, cyanuric acid production needs to be developed by using a facile protocol. Traditionally urea pyrolysis is utilized to produce cyanuric acid. The utilization of sulfuric acid is one of the drawbacks of the current procedure. We proposed to use for the first time exploiting low-cost Brønsted ionic liquid as a catalyst and solvent system for effective production of cyanuric acid. The reaction time and temperature were reduced compared to the previous studies. DFT was applied to compute the reaction mechanism and to generate a lower energy route that yields cyanuric acid. The ionic liquid catalyzed route was matched with a catalyst-free route to see the catalyst's role in decreasing energy barriers. Using computational tools, we identified that the reaction was more likely to undergo via in-situ generation of isocyanic acid and its immediate trimerization to cyanuric acid. We decided the study can contribute to overcoming challenges in urea pyrolysis to cyanuric acid. Industrially applicable value-added product formation using CO_2 as a starting material contributes to maintaining

a net-zero goal. Developing a method for utilizing CO_2 carbon as building blocks for organic feedstock supports sustainable development and, eventually, the world's clean future. To meet the goal, we computationally investigated the cyclocondensation reaction of CO_2 with various nucleophilic substrates, such as ethylenediamine, ethylene glycol, and ethanolamine. Because of the importance, the target reactions were conducted experimentally in harsh conditions with non-benign catalysts. Our calculations showed that the target reactions could be modified according to the 'green' requirements. Unlike the experimental procedure, we suggested the utilization of low-cost Brønsted acidic ionic liquids as a 'greener' catalyst for the considered reaction. The free energy surface described two concerted transition states: CO_2 binding and ring closure and dehydration steps to reach heterocyclic carbonyl derivatives. Computations suggested that the CO_2 binding step is almost barrierless, while ring closure and dehydration require 32.8 kcal/mol energy to yield the product in the case of ethylenediamine is taken as a substrate. The utilization of various substrates and catalyst (ionic liquid) variants for CO_2 conversion generated a map that helps experimentalists conduct a greener reaction to convert CO_2 according to the proposed methodology.

The practical importance of the work. Computational simulations help to optimize a reaction intermediates and transition states to design a PES, which can be exploited to predict the feasibility of a reaction, so it supports to prevent time and material consumption in a lab. DFT calculations shown in the proposed research are a valuable contribution to smart catalyst development, which can be proposed as an alternative to the currently used catalyst applied in the industry. Recent investigations showed that experimental and DFT studies are in good agreement (>90 %).

Published scientific works. The materials related to the dissertation have been published in a total of 31 scientific publications. Notably, 15 manuscripts were published in reputable journals with high impact factors, all of which are indexed in the Web of Science and Scopus databases. Additionally, 9 manuscripts found their place in local journals, with 5 of them being single-authored. The remaining

7 publications took the form of conference proceedings or abstracts presented at both local and international conferences.

Approbation of the work. The dissertation results have been discussed in the following conferences: Conference on Environmental Remediation Granada (Spain) - May 26-27, 2022, 5th Green and Sustainable Chemistry Conference, 10-11 November, 2020, Dresden, Germany. 1st International Congress on Natural Sciences (ICNAS-2021), 10-12 September 2021, Atatürk University, Erzurum, Turkey. 15th Tetrahedron Symposium Challenging in Bioorganic and Organic Medicinal Chemistry 24-27 June 2014 London.

The name of organization the works in dissertation carried out. The proposed dissertation was carried out according to the scientific direction of the Lab # 24 of the Institute of Petrochemical Processes named after Y. Mammadaliyev

The dissertation volume and structure. The dissertation consists of a table of contents, acronyms, three chapters, conclusions, references, and an appendix. The dissertation materials are 281 pages, which include 16 tables, 93 figures, 31 schemes, and 407 references. **The introduction** section consists of 33752 characters and includes relevance, purpose, novelty, and practical importance of the work.

Chapter 1 includes (53659 characters) introductions related to pyrrolo-triazepine derivatives availability in nature, other synthetic strategies for the synthesis of similar compounds, and pharmaceutical application of the related scaffolds.

Introduction about polycyclic imidazole synthesis and application as biologically active compounds. Screening of the previous methodologies about multisubstituted imidazole synthesis and application. The role of IL in imidazole synthesis as a catalyst and solvent system was also added to Chapter I. Previous computational approaches were also discussed in the chapter. $C(sp^3)$-H activated imidazole synthesis was reviewed in Chapter I. IL mediated azo-group containing imidazole synthesis was reviewed. Literature review about triazinane and triazinane-2-thion derivatives synthesis and application was included. Literature studies related to vegetable oil epoxidation and subsequent aminolysis were added. Previously utilized catalysts

were reviewed and compared to the catalyst utilized in our computational studies. Past experimental and computational methodologies related to biomass, in particular, glucose conversion to 5-HMF were mentioned. The pros and cons of the previously utilized catalysts were discussed. The advantages of using IL-based catalysts were stated. p-phenylenediamine polymerization to poly-p-PDA was reviewed, and the urgent need to the application of computational studies to the polymerization reaction mechanism elucidation was stated since disagreement existed among experimental polymer scientists on the hypothesized polymerization mechanism. Cyanuric acid synthesis and utilization as a precursor to synthesize new generation disinfectants (trichloroisocyanuric acid, sodium dichloroisocyanuric acid) production was discussed. Previous literature studies were included related to cyanuric acid and its derivatives. The importance of carbon dioxide conversion to value-added organic chemicals was stated. Past computational and experimental approaches in carbon dioxide conversion to heterocyclic carbonyl derivatives were mentioned.

Chapter 2 consists (148201 characters) synthesis of 5H-pyrrolo[2.1-d][1,2,5]triazepine derivatives started from pyrrole. The target product synthesis followed three-step process; first, pyrrole conversion to pyrrolecarbaldehyde or ketone via utilizing $POCl_3/RCONMe_2$ system. Second, treatment of pyrrolecarbaldehyde with propargyl bromide in the presence NaH/DMF resulted in the hydrogen (attached to the pyrrole N atom) substitution with propargyl group. Third, the resultant compound was treated with hydrazine monohydrate in the reflux condition with methanol, yielding fused pyrrolotriazepine derivatives. Propargyl-allene isomerization, cyclization, and the reaction of hydrazine steps were studied computationally.

One-pot four components tetrasubsituted imidazole synthesis from benzil, ethanolamine, ammonium acetate, and various benzaldehyde derivatives were studied experimentally and theoretically. The role of IL in the quantitative synthesis of product was determined. The reaction was simulated three times in IL-free, IL-solvation, IL-catalysis conditions. Theoretical TOF analysis was

applied to determine the best route for the one-pot multisubstituted imidazole synthesis. Three polycyclic aromatic imidazole derivatives 2-phenyl-1-(4-(phenyldiazenyl)phenyl)-1H-phenanthro[9,10-d]imidazole, 2-(4-methoxyphenyl)-1-(4-(phenyldiazenyl)phenyl)-1H-phenanthro[9,10-d]imidazole, 2-(2,4-dichlorophenyl)-1-(4-(phenyldiazenyl)phenyl)-1H-phenanthro[9,10-d]imidazole are synthesized with one-pot four component fusion reaction using 1,4-dimethylpyperazinium dihydrosulfate IL. The mechanism of the cyclocondensation reaction was elucidated with DFT studies. TD-DFT analysis was conducted to determine HOMO-LUMO energy gap energies.

$C(sp^3)$–H activated two-components metal- and solvent-free cyclization to multisubstituted imidazole and pyrazine was studied experimentally and computationally.

The plausible mechanism was computed for acetic acid and its trichloro- and trifluoro- versions catalytic effects on thiourea, ammonia, and benzaldehyde fusion to (4S,6S)-4,6-diphenyl-1,3,5-triazinane-2-thione.

Computational approaches on the vegetable oil C=C double bond defunctionalization and subsequent aminolysis were discussed. $FeCl_2$, $ZnCl_2$, and $NiCl_2$ Lewis acidic salt catalysts application on epoxide ring opening were elucidated. Regardless of the regular exploitation of $ZnCl_2$ in practice, our computations recommend that $FeCl_2$ would be a better catalyst based on the calculated energetic span.

Biomass conversion to 5-HMF was studied experimentally and computationally using low-cost and readily available IL catalysts. Screening of Lewis and Brønsted acidic catalysts on the reaction showed that the utilized IL catalyst is superior because of its unique features, e.g., the IL catalyst cation part bearing two catalytic centers which hold glucose molecule for effective dehydration.

Mechanistic studies were conducted on persulfate-initiated p-phenylenediamine polymerization to poly-p-PDA. Sulfate free-radical, persulfate anion, and potassium persulfate cluster-initiated polymerization routes were computed. The potassium persulfate cluster promoted route energy barriers were found to be very shallow compared other two routes.

Cyanuric acid synthesis from urea was studied experimentally and computationally. The reaction was optimized based on various parameters (e.g., time, temperature, solvent, and catalyst loading). Eight different ILs were tested on the reaction, and dimethylammonium hydrosulfate was selected as the best IL for further optimizations. Mechanistic studies confirmed that urea pyrolysis resulted in isocyanic acid, which can easily trimerize into cyanuric acid in the presence of IL catalytic conditions with shallow energy barriers.

Carbon dioxide conversion to the five-membered heterocyclic carbonyl derivatives was conducted computationally. Computational studies suggested that ethylene diamine is the best substrate for effective carbon dioxide conversion. Attaching electron donating and withdrawing groups to ethylenediamine does not reduce the energy barriers. Altering IL via replacing the anion component (HSO_4^-) central S atom with 6 A and 5 A group elements (Se, P, and As) demonstrate that Se-based IL can act similarly to hydrosulfate. Molecular dynamics (MD) simulations show that the IL ion pairs can catch substrate and carbon dioxide molecules via noncovalent interactions to facilitate a nucleophilic attack on carbon dioxide.

Computational studies were performed in density functional theory (DFT) B3LYP/6-31G* level of theory for optimizing the synthesized surfactant structures and determining their formation-free energies.

Chapter 3 comprises (71351 characters) experimental and computational methodologies for the synthesis of triazepine derivatives, polycyclic imidazoles, triazinane-2-thione, vegetable oil epoxidation and aminolysis, 5-HMF, poly-p-PDA, IL-mediated urea conversion to cyanuric acid, and computational predictions regarding carbon dioxide conversion to heterocyclic carbonyl derivatives.

Conclusion section consists (18199 characters) of main computational and experimental results and prospectives.

The applicant contribution in the carried out works. Literature review, writing of dissertation, lab experiments, spectroscopic structure elucidation, and utilization of computer software for the theoretical studies were conducted by author.

17

Brief information of the work (Synopsis)

Nitrogen-containing heterocyclic organic compounds have always been a focus for scientists due to their pharmaceutical applications. Nevertheless, there is a need for in-depth exploration of computational mechanistic studies related to their synthesis. In line with this, we have investigated the mechanisms behind the synthesis of nitrogen-containing biofuels, drug agents, and lubricants, which significantly contributes to the development of synthetic procedures. Through quantum calculations, we have obtained Gibbs energy profiles and computational TOF values, which support the matching of homogeneous catalysts and offer an opportunity to identify the best catalyst for a given reaction.

1. Synthesis and theoretical mechanistic studies of pyrrolotriazepine derivatives.

Our planned approach to **10** involved metal-free cyclization of pyrrole hydrazone derivatives **11**, synthesized by the reaction of acylpyrroles **12** having an alkyne moiety attached to the nitrogen atom of pyrrole with hydrazine. The retrosynthesis is summarized in Scheme 1.1
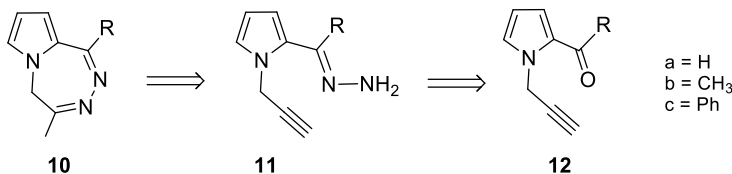
Scheme 1.1. Retrosynthesis of pyrrolotriazepine derivatives

For the synthesis of pyrrole-fused triazepine derivatives, the starting materials were prepared according to the literature. Pyrrole carbonyl compounds were prepared by application of the Vilsmeier reaction, which is an alternative to Friedel-Crafts acylation and avoids the use of strong Lewis acids such as $AlCl_3$. This method is particularly useful for the formylation of electron rich aromatic compounds such as pyrrole with substituted amide and phosphorus oxychloride to produce pyrrolecarbaldehyde or ketone. As depicted in the following scheme (Scheme 1.2), treatment of the heterocyclic building blocks **14a-c** with propargyl bromide afforded the alkyne derivatives **12a-c**.
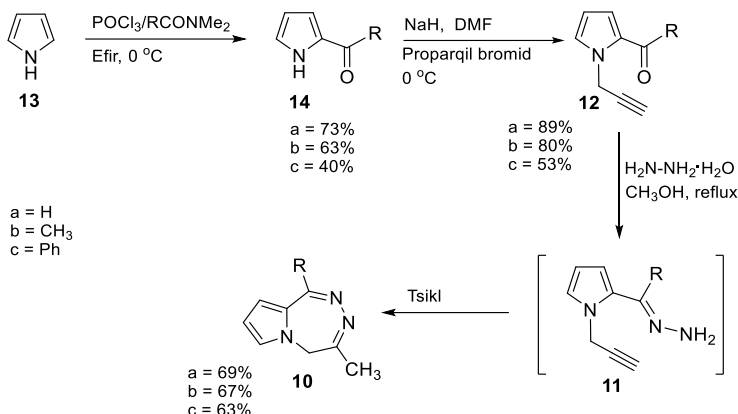
Scheme 2.2. Synthesis of pyrrole fused triazepine derivatives

To the best of our knowledge, the facile construction of this new pyrrole-fused triazepine skeleton has not been previously explored. Heating of synthesized propargyl derivatives 12a-c with hydrazine monohydrate in methanol at reflux temperature produced the desired cyclization products 10a-c, which were isolated in good yields (63-69%) after chromatographic purification.

2. Multisubstituted imidazole synthesis and theoretical studies: Identification of the catalytic and solvation features of IL[ET$_2$NH$_2$][HSO$_4$]

Herein, we would like to establish a clear distinction between the IL aiding a reaction as a solvent, as compared to acting as a catalyst. [Et$_2$NH$_2$][HSO$_4$] was used to synthesize 2-(2,4,5-triphenyl-1H-imidazolium-1-yl)ethan-1-ol from the four components (benzil, ethanolamine (ETA), ammonium acetate, benzaldehyde) cyclocondensation reaction according to the following scheme (Scheme 2.1):
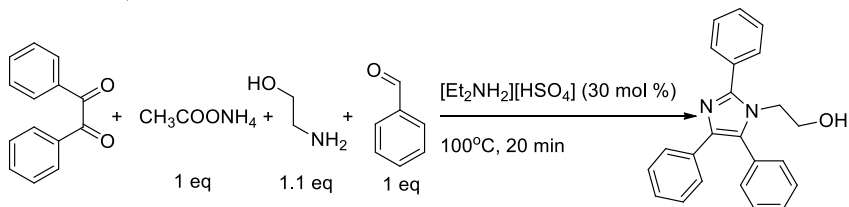
Scheme 2.1. [Et$_2$NH$_2$][HSO$_4$] promoted synthesis of 2-(2,4,5-triphenyl-1H-imidazolium-1-yl)ethan-1-ol.

As seen from Table 2.1, through utilizing various benzaldehyde derivatives several multicomponent imidazole derivatives (2a—j) were synthesized.

Table 2.1: The reaction time, yield of (**2a—j**) products and related melting points.

№	R	mp (ºC)	Time (min)	Yield (%)	Mol. formula (mol. mass)
2a	H-	184-185	20	98	C$_{23}$H$_{20}$N$_2$O (340.42)
2b	2-OH	108-110	25	92	C$_{23}$H$_{20}$N$_2$O$_2$ (356.42)
2c	4-OH-	287-289	15	92	C$_{23}$H$_{20}$N$_2$O$_2$ (356.42)
2d	3-OCH$_3$	160-162	35	82	C$_{24}$H$_{22}$N$_2$O$_2$ (374.86)
2e	4-OCH$_3$-	187-188	30	95	C$_{24}$H$_{22}$N$_2$O$_2$ (370.44)
2f	2,4-CH$_3$O-	175-177	30	88	C$_{25}$H$_{24}$N$_2$O$_3$ (400.47)
2g	3,4-CH$_3$O-	212-214	35	92	C$_{25}$H$_{24}$N$_2$O$_3$ (400.47)
2h	2,5-OCH$_3$-	198-200	35	92	C$_{25}$H$_{24}$N$_2$O$_3$ (400.47)
2i	4-(CH$_3$)$_2$N-	207-209	35	93	C$_{25}$H$_{25}$N$_3$O (383.49)
2j	4-NO$_2$-	190-192	15	85	C$_{23}$H$_{19}$N$_3$O$_3$ (385.42)

We chose benzaldehyde among the array of aldehydes that were used in our experimental work because of its simple structure, along with other reagents, namely benzil, ethanolamine, ammonium acetate, and [Et$_2$NH$_2$][HSO$_4$], to conduct theoretical calculations on the reaction.

The one-pot synthesis of substituted imidazoles is also a suitable example representing more general nucleophilic addition and cyclocondensation reactions. Brønsted acidic ILs are the best example for proton exchange according to the following scheme (Scheme 2.2):
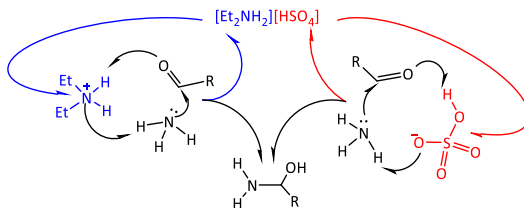
Scheme 2.2. Cationic and anionic components of IL dual catalytic effect on nucleophilic addition.

Brønsted acidic ILs are perfect agents for proton exchange (see Scheme 2.2) in a nucleophilic addition reaction. $[HSO_4]^-$ may act as a proton donor and it was hypothesized in a recent study that it may also act as a proton acceptor as the anionic component of 2-ethyl imidazolium hydrogen sulfate. $[HSO_4]^-$ as the acidic component of the IL can donate a proton to the carbonyl containing species rather easily to become $[SO_4]^{2-}$ which may then accept a proton from a nucleophile (ammonia or benzyl amine in this study), and convert back to hydrosulfate. Strong acids, such as H_2SO_4 are not capable to perform in the same way. In the H_2SO_4 case, there is a low concentration of proton acceptors in the medium to catalyze the reaction as well as the IL does. The cationic component of the ionic liquid, $[Et_2NH_2]^+$, can act in a similar way in the reaction of Scheme 2.1, e.g. by donating a proton to carbonyl, becoming a strong base, and easily abstracting a proton from ammonia interacting with the electropositive carbon. Our computations reveal that the anionic and the cationic component of the IL together cause a `*dual effect*' of catalyzing the multisubstituted imidazole synthesis reaction. The effects from the IL acting as a solvent are also investigated and described.

Computational studies: Under the reaction conditions, ammonium acetate is decomposed and ammonia reacts directly with carbonyl species (benzil, benzaldehyde). Nucleophiles and carbonyl-containing species in these one-pot conditions imply four possible interactions for

the starting point of the reaction: ammonia+benzaldehyde, ammonia+benzil, ETA+benzaldehyde, and ETA+benzil. Hence, ammonia coming from ammonium acetate is only thought to be present as a nucleophile and acetic acid may act as a solvent. We calculated the reaction steps twice, first in the gas phase and then with a solvent model for AcOH, starting with the ETA+benzil interaction (see the Supporting Information). Based on the energy barriers, AcOH as a solvent is not a deciding factor in rendering the reaction more feasible. Moreover, in the gas phase, this route turned out to afford high-energy barriers compared to the route that starts with an ammonia+benzaldehyde interaction. Hence, we decided to proceed with the ammonia+benzaldeyde interaction as a starting point to identify IL effects on the whole reaction profile. Both molecules are relatively small and the probability of reactive collisions among them was deemed more likely compared to the other starting possibilities. Moreover, the reaction route starting with the ETA+benzaldehyde interaction is the same as the calculated ammonia+benzaldehyde route after the diamine formation (Figure 2.1)
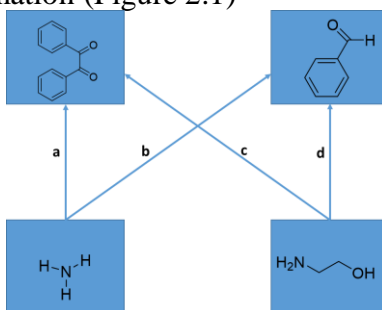
Figure 2.1. Interaction possibilities of the starting compounds.

The reaction steps were calculated in three different ways in order to obtain reaction profiles free of interactions with the IL, with IL solvation, and with the IL being catalytically active.
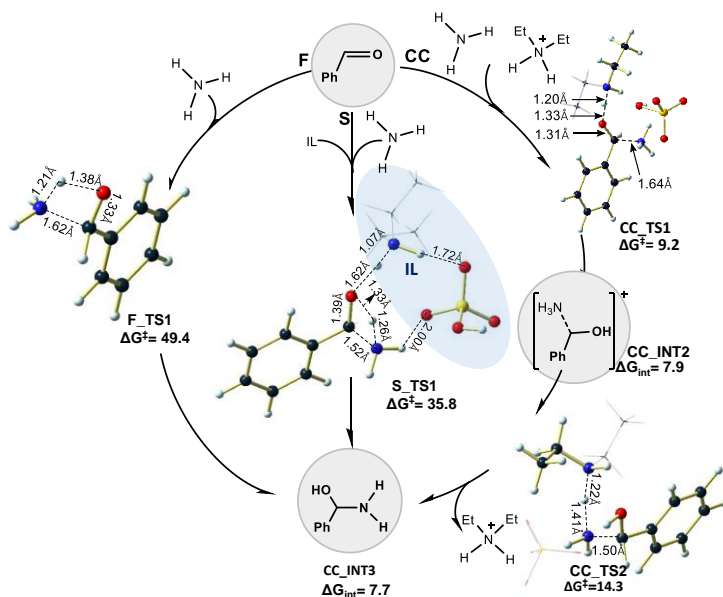
Figure 2.2. Calculated mechanisms for the amino(phenyl)methanol formation step. **F**: IL-free route. **S**: IL-solvation route. **CC**:

IL-Catalysis (C): We tested the amino(phenyl)methanol formation path of figure 2, but now allowing for proton transfer between the IL and other species present. Remarkably, proton transfer between IL and carbonyl or amine functional groups in the transition states strongly lowers the energy barriers compared to the IL solvation route. The amino(phenyl)methanol formation path was calculated twice, with $[Et_2NH_2]^+$ and $[HSO_4]^-$ incorporation, respectively. The IL catalytic effect takes place via proton exchange between the cationic and anionic components of the IL and carbonyl, amine, and hydroxyl functional groups, which is evidently different from the IL-solvation effect.

$([Et_2NH_2]^+)$ catalytic route. Transition states $(\Delta G^{\ddagger})$ and intermediates (ΔG_{int}) Gibbs free energies and transition state optimized structures with important bond lengths are added to the figure.

[Et₂NH₂]⁺ Incorporation: Figure 2.2 compares the **F**, **S**, and the IL cation catalysis (**CC**) variants of the amino(phenyl)methanol

formation. This reaction step would require 49.4 kcal/mol activation energy in the **F** route, and 35.8 kcal/mol in the **S** route. In the **CC** route, $[Et_2NH_2]^+$ readily shares a proton with the carbonyl oxygen. The corresponding transition state **CC_TS1** and is calculated to be only 9.2 kcal/mol higher in energy than the starting materials. The subsequent deprotonation of ammonia in order to reach the amino(phenyl)methanol intermediate product has an even smaller barrier of 6.4 kcal/mol (**CC_TS2**) relative to the intermediate. Figure 2.3 continues the comparison of the **S** and **CC** routes.
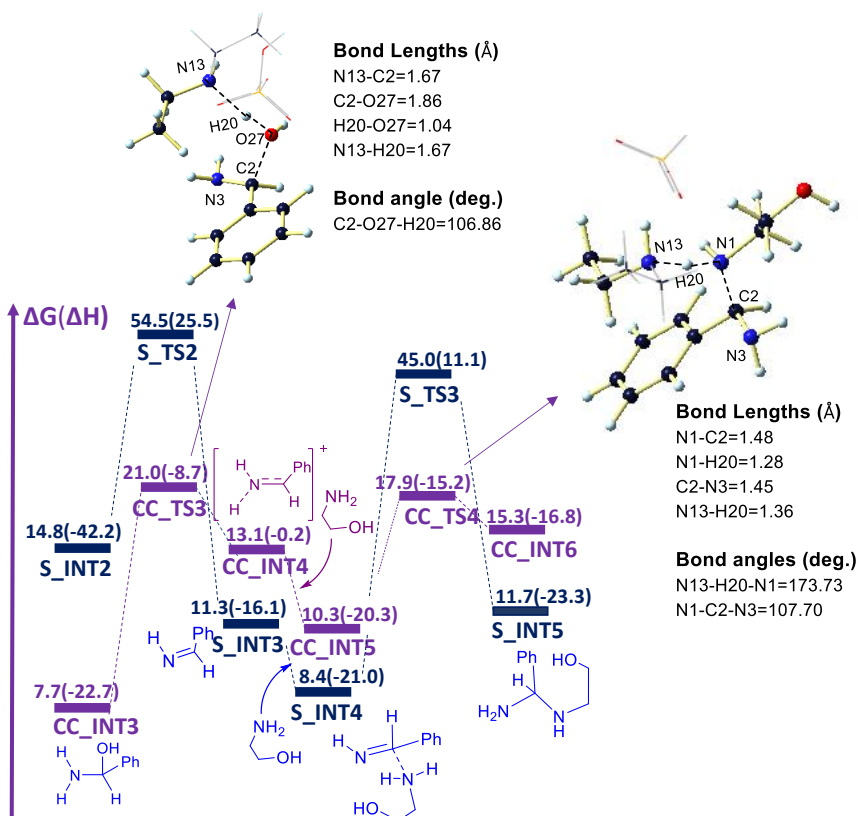
Figure 2.3. The diamine formation step based on the (purple) IL cation incorporation in the transition states. For comparison, the IL solvation

path (dark blue) is included in the figure. In the **C_TS3** and **C_TS4** structures, Et- groups of $[Et_2NH_2]^+$, and $[HSO_4]^-$ are omitted for the sake of clarity.

The main difference between them is that **CC_INT4** is the imine cation (a natural bond orbital (NBO) analysis clearly indicates the presence of a localized C=N double bond) stabilized by the polar environment, while **S_INT3** is a neutral imine intermediate. The latter is lower in energy, but its formation has a higher barrier. Further addition of ETA via the **S** path also affords a considerably higher barrier. In the catalytic route up to the diamine formation (**S_INT5**), the hydroxylation and dehydration steps afford higher barriers than the deprotonation steps and can be considered as rate-determining up to this point in the reaction.

What renders the **CC** route more feasible? For instance, the **CC** transition states in the amino(phenyl)methanol formation step are overall different from the **F** and **S** routes because of the separate hydroxylation and deprotonation steps, which evidently requires less activation energy overall. To see why, we turn to the optimized transition state structures in Figure 2.2 and 2.3 in order to scrutinize the bond distances. In Figure 2.2, the **F_TS1**, **S_TS1**, and **CC_TS1** structures exhibit important differences. In the **F** and **S** routes, the benzaldehyde carbonyl bond elongates more compared to the **CC** transition states, which is for the most part associated with an energetic penalty.

The optimized benzaldehyde carbonyl bond distance is 1.22Å. In **F_TS1**, the carbonyl bond is stretched to 1.33Å, and even further in **S_TS1** (1.39Å) which is assisted by a balancing stabilization from the hydrogen bonding network. In **CC_TS1** the corresponding distance is 1.31Å (Figure 2.2). The IL cation transfers the proton to the carbonyl oxygen without elongating the carbonyl double bond too much. The follow-up transfer of a proton back to the IL is accomplished with little of a barrier.

3. Metal-free and BrØnsted acidic ionic liquid catalyzed C(sp³)-H activated multisubstituted imidazole and pyrazine synthesis from benzil and benzylamine.

Herein, we propose an atom economic, solvent- and metal-free, one-step protocol for the synthesis of multisubstituted imidazole and pyrazine rings. We also optimized the benzil and benzylamine reaction conditions for the **PRO1** and **PRO2** yield to a remarkable level (Scheme 3.1).

Five factors such as the type of IL, reaction temperature, time, solvent, catalyst loading, which influence the reaction yield were optimized. The highest yield of **PRO1** does not exceed 29% in the presence of n-BuOH as a solvent while **PRO2** formation is not observed.
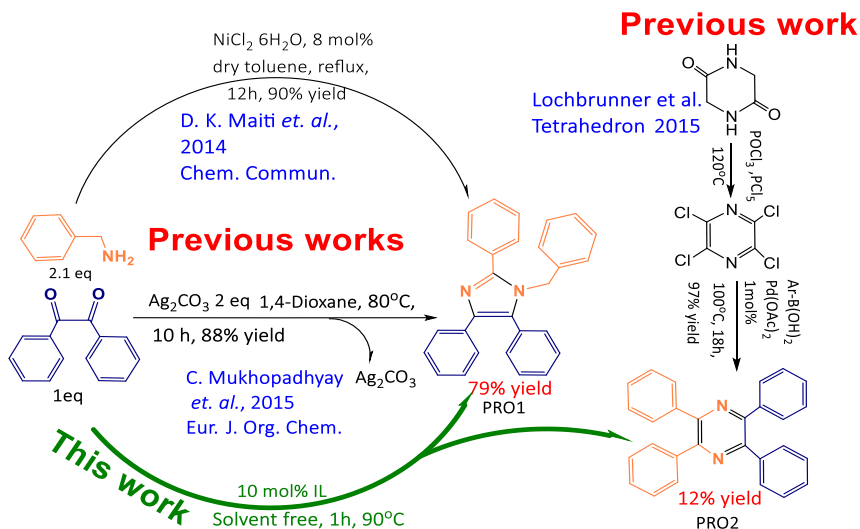
Scheme 3.1. IL (this work) and metal (previous works) catalyzed C-H activated annulation reactions.

Conversely, in the presence of DMSO the **PRO2** yield reaches the highest value (54%) while the **PRO1** yield is only 7%. All other reaction parameters were the same as under solvent-free conditions. Other tested solvents (DMA, DMF, pyridine, water, glycerol, toluene, 1.4-dioxane) performed less effective than DMSO and n-BuOH

regarding the product formation. With solvents, the highest **PRO1** yield (in the presence of n-BuOH) is nearly three times lower than the highest yield under solvent-free conditions. Despite the **PRO2** yield being higher in the presence of DMSO, the combined product yield does not exceed 61%. In the solvent-free condition, 79% yield of **PRO1** is obtained. We also optimized **PRO2** formation in the solvent-free condition (See Scheme 3.1) to a level that is as high as in the presence of DMSO.   This investigation shows that solvent-free conditions are not only feasible but in fact favorable for the synthesis of **PRO1** and **PRO2**. Accordingly, further investigations have been carried out under solvent-free conditions. These conditions are also desirable because of "green" aspects. A variety of products can be synthesized with the same procedure.

Variation of IL: The **PRO1** and **PRO2** (byproduct) formation reaction from benzylamine ($BnNH_2$) and benzil is studied after 1 hour at 90ºC in the presence of various (10 mol%) ILs as a catalyst. Without an IL catalyst, much less conversion of substrates to **PRO1** and **PRO2** is observed. The best results are achieved in the presence of $[taH_4][I_4]$ and $[deaH][HSO_4]$. $[taH_4][I_4]$ holds four amphiprotic centers (NH^+), and they actively take part in the protonation and dehydration steps of the annulation reaction. Further optimizations were carried out at the presence of $[deaH][HSO_4]$ as a catalyst because of satisfactory yield of **PRO1** and easy access to this catalyst.

Variation of the reaction time: The first set of reactions were performed at 90 °C with varying reaction times to obtain an indication of reaction rate. Figure 1 illustrates the yields of the two products versus time in the presence of 10 mol% catalyst $[deaH][HSO_4]$ at 90 °C. According to the graph the maximum yield for **PRO1** is obtained at 1 hour. During the first 60 minutes the **PRO1** yield increased up to 75% whereas the **PRO2** yield is trace 18%. Increasing reaction time shows decreased conversion to **PRO1** with increasing **PRO2** formation. After about 3 hours, the **PRO2** yield becomes greater than **PRO1**. The product formation does not change much after about 6 hours. This investigation shows that the **PRO1** vs. **PRO2** yield is strongly time dependent, such that the products formation can be tuned via time. Effective heating over a long time facilitates $C(sp^3)$-H

27

activation and the subsequent C-C cross-coupling which is not the catalyst dependent (it binds to the substrate proton via hydrogen bonding, See Figure 3.6, **TS1-PRO2**) yields the six-membered dihydropyrazine ring (**INT2-PRO2**). Experimental investigation shows that 1 h is not enough to finalize the reaction with full annulation to the pyrazine ring via multi-step processes (e.g. bond activation, cross-coupling, deprotonation of the **INT2-PRO2**).
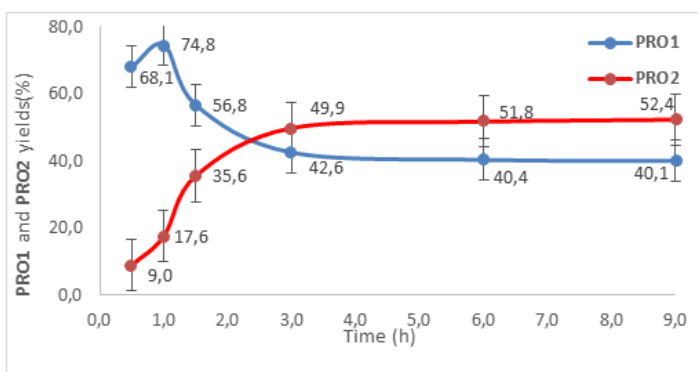

Figure 3.1. PRO1 and **PRO2** formation versus time at 90 °C in 10 mol% catalyst [deaH][HSO$_4$] loading.

Variation of [deaH][HSO$_4$] catalyst loading:
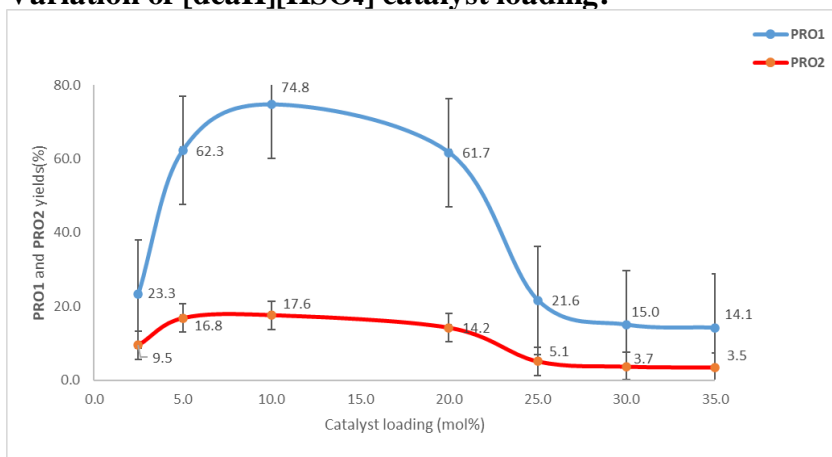
Figure 3.2. Yields of **PRO1** and **PRO2** versus [deaH][HSO$_4$] concentration at 90 °C after 1 hour.

The relation between different catalyst loadings of [deaH][HSO₄] and product yields after 1 hour of reaction time is given in Figure 3.1. As seen from the figure, conversion to the products starts to decrease sharply at 20 mol% catalyst loading. This point is taken to be the concentration at which the IL turns to act as a solvent. The highest yields of the products are achieved with 10 mol% of the IL, which is therefore an optimized concentration for the IL used for subsequent reactions. IL solvation versus catalysis was studied extensively in our previous computational work. Calculated energy barriers were observed to be lower in case of proton exchange between a substrate and a catalyst molecule. The IL interaction with the substrate molecule via hydrogen bonding decreases the energy barriers as well, but it was higher than the IL proton exchange case (catalytic). Intermolecular hydrogen bonding and other electrostatic interactions between the IL molecules increase solvation ability when IL is bulk (20 mol% and more). In a lower concentration (10 mol% and less) IL molecules don't likely colliding with each other and that increases the probability of proton transfer between IL and a substrate molecule which increases catalytic performance.

Variation of the reaction temperature:
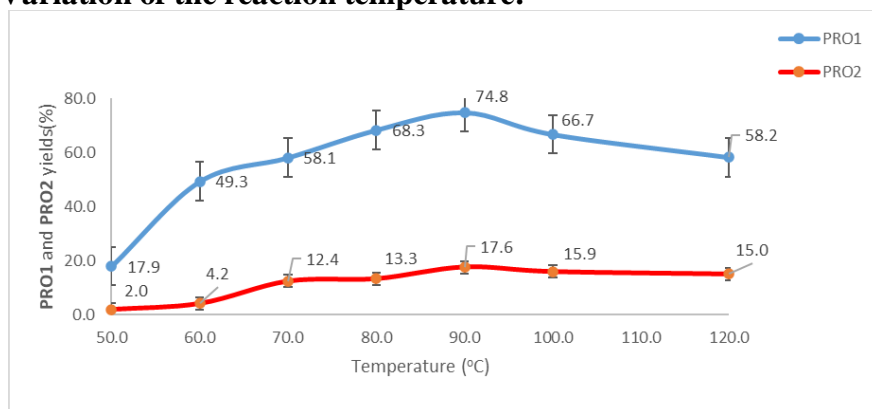
Figure 3.3. The yield of **PRO1** and **PRO2** versus temperature. Conditions: 10 mol% [deaH][HSO₄], 1 hour.

The reaction is conducted at different temperatures in the presence of 10 mol% [deaH][HSO₄] in 1-hour period Figure 3.3). The yield of

PRO1 increased with increasing temperature up to 90 °C, beyond which the **PRO1** formation declines significantly. At the lower temperatures (50-60 °C), **PRO2** formation is hardly noticeable and it remains relatively constant over the temperature range 70 -120°C. The decrease in **PRO1** formation beyond 90°C can be scrutinized with the catalyst deactivation: The $[Et_2NH_2^+]$ proton transfer to a substrate may yield the diethylamine moiety. We studied previously 'dual' catalytic activities of the cationic and anionic parts of the IL in the proton exchange. This is a volatile liquid (b.p. is 55°C), and at the tested temperatures it may result in the catalyst mass loss.

Recycle test: Figure shows that the catalyst is effective over three reuses without significant decline in the **PRO1** yield. The recycle test also is in good agreement with the data in Figure 3.4. **PRO2** formation does not change much over 8 reuses. This seems to suggests that **PRO2** formation is not much catalyst dependent within a short (1 hour) reaction time. However, according to the theoretical mechanistic study in the following section, two subsequent transition states in the **PRO2** formation play a crucial role for the formation of the 6-membered heterocycle. The catalyst becomes active in the proton removal that results in the pyrazine ring formation (see **PRO2** formation pathway in Figure 3.5). For long reaction times, the catalyst shifts the reaction toward **PRO2**.

	1	2	3	4	5	6	7	8
PRO1	74.8%	74.7%	69.0%	43.0%	43.0%	39.0%	30.0%	22.0%
PRO2	17.6%	17.3%	17.3%	16.9%	16.4%	16.2%	16.0%	14.8%

Number of recycles
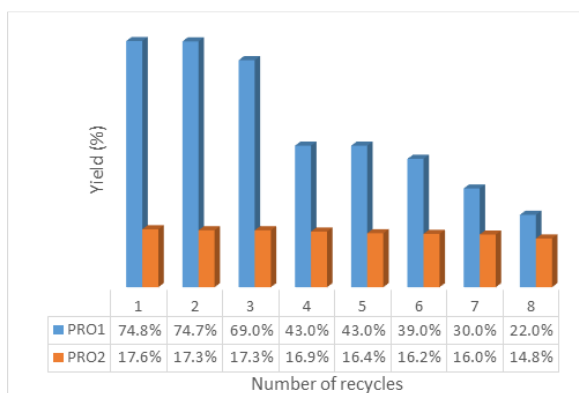
Figure 3.4. Recycle test of IL: benzil (2.50 mmol), benzylamine (5.50 mmol), and 10 mol% of [deaH][HSO4] at 90°C in 1 h.

Computational Mechanistic details: A detailed computational investigation of the reaction leading to **PRO1** was carried out and produced the reaction profile shown in Figure 3.5. The $BnNH_2$ and benzil interaction yields a diimine intermediate which is converted to the final product through $C(sp^3)$–H activation (See Scheme 3.2). The $BnNH_2$ and benzil interaction gives 2-(benzylamino)-2-hydroxy-1,2-diphenylethan-1-one (**INT2**) via **TS1** which is calculated to be 15.2 kcal above the starting materials. **TS1** is a concerted transition state: proton exchange (HSO_4^- is donating its proton to the carbonyl oxygen and getting proton from $BnNH_2$ at the same time) results in the **INT2** formation. Selected bond distances of the **TS1** for the proton exchange are given in Figure 3.6. The IL cation component is in close proximity (N-H: $1.08A^o$ and O-H: $1.59A^o$) to the anion component and acts as a supporter in the proton transformation.
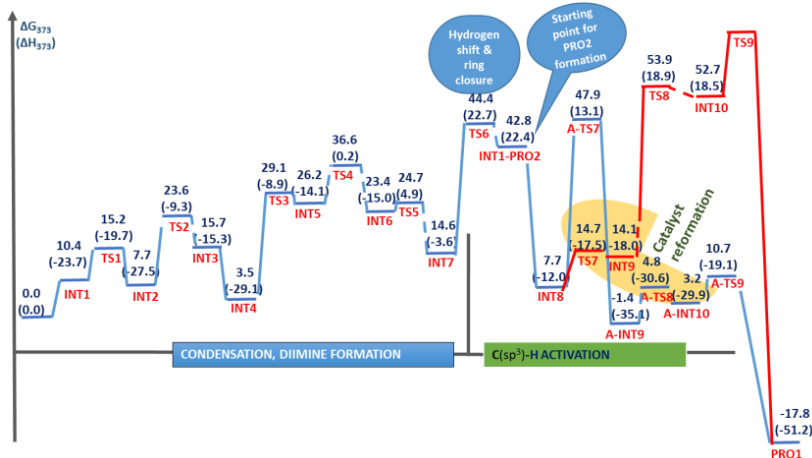
Figure 3.5. Reaction profile (kcal/mol) for the C-H activated annulation reaction according to DFT calculations.

These kinds of concerted TSs were located for further dehydration (**TS2**) and protonation (**TS3**) steps. The next step via **TS2** with a 15.9 kcal barrier yields water abstraction. Addition of the second $BnNH_2$ molecule to the imine (**INT3**) produces a diimine (**INT7**) via the protonation of the second carbonyl of the benzil and dehydration (**INT4→INT7**) of **INT5**. The next part (**INT7→PRO1**) of the

31

reaction constitutes the C(sp^3)–H bond activated annulation of the **INT7** to **PRO1** and **PRO2**.
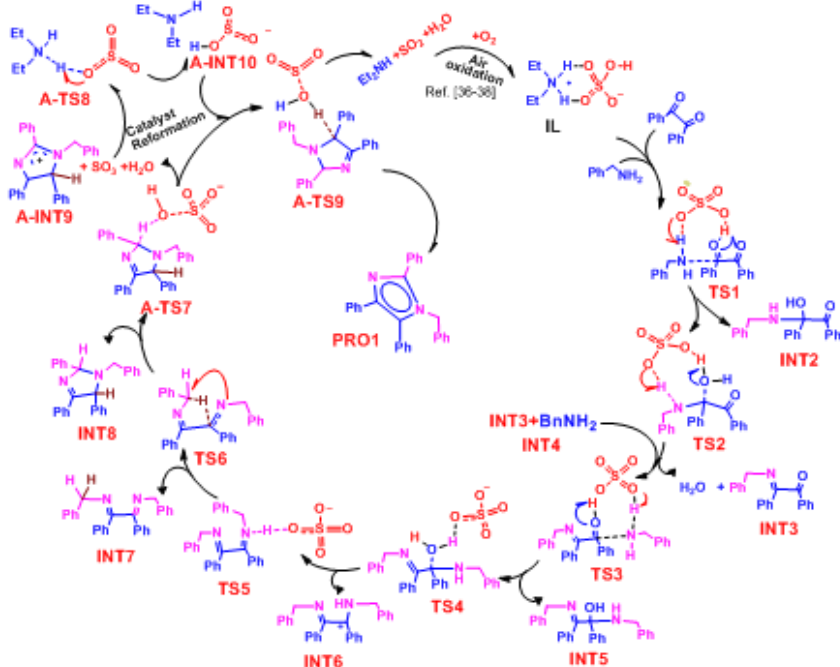
Scheme 3.2. **PRO1** formation mechanism according to the blue route of Figure3.5. The IL cation part is omitted in some transition state structures for clarity.

The IL cation and anion components are not catalytically active in the hydrogen shift in **TS6** (See Figure 3.6). The cation component connects with nitrogen (**6**) via hydrogen bonding. The hydrogen shift transition state is calculated to have a high barrier (29.8 kcal) compared to the condensation route energy barriers. It is playing a key role in the **PRO1** and **PRO2** formation steps. **TS6** leads to benzylic C**2**(sp^3)–H**1** bond cleavage and subsequent proton (**1**) migration renders (C**5**=N**6**) the imine C**5** (sp^2) saturation. It follows through the electron reach nitrogen (**6**) attack to benzylic C(sp^2) yields the C**2**–N**6** cross-coupling type cyclization intermediate (**INT8**). Further proton abstraction on the five-membered ring via sulfate reduction was investigated because the above mentioned alternative reaction

pathways could not be accepted as plausible routes for **PRO1** formation.
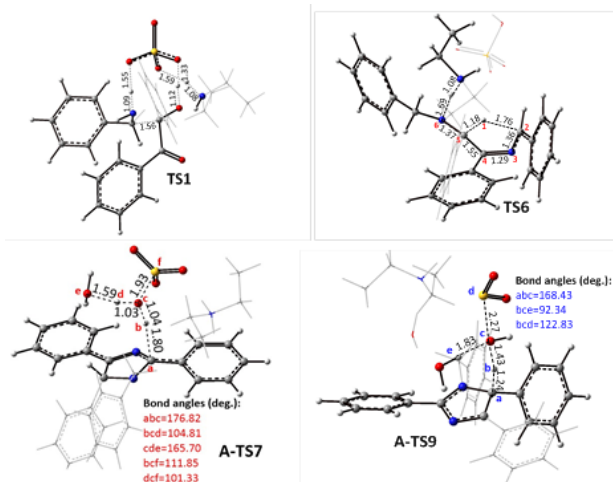
Figure 3.6. The optimized structures of **TS1, TS6** (the hydrogen shift TS), **A-TS7**, and **A-TS9** with important bond lengths (given in Å), and angles (deg.). $[Et_2NH_2]^+$, $[HSO_4]^-$, and Ph groups are omitted for clarity.

TS6 leads to benzylic $C2(sp^3)$–H**1** bond cleavage and subsequent proton (**1**) migration renders (C**5**=N**6**) the imine C**5** (sp^2) saturation. It follows through the electron reach nitrogen (**6**) attack to benzylic $C(sp^2)$ yields the C**2**–N**6** cross-coupling type cyclization intermediate (**INT8**). Further proton abstraction on the five-membered ring via sulfate reduction was investigated because the above mentioned alternative reaction pathways could not be accepted as plausible routes for **PRO1** formation.

The $C(sp^3)$-H activation steps lead to the product in one of two ways: The catalyst reformation and sulfuric acid dehydrsoxylation (reduction) or hydrosulfate reduction to sulfur dioxide.

4. CX₃COOH (X=F, Cl, H) catalyzed synthesis of triazinane derivatives and related computational mechanistic studies.

As a model reaction, the one-pot three-component (OTC) synthesis of (4S,6S)-4,6-diphenyl-1,3,5-triazinane-2-thione from ammonia, benzaldehyde, and thiourea is considered. Simple starting materials are chosen to investigate the reaction mechanism at the Kohn–Sham (KS) DFT level (Scheme 4.1):
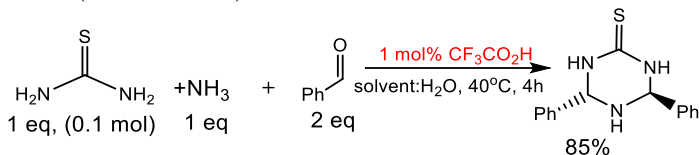
Scheme 4.1. The reaction considered in the quantum chemical calculations.

Discussion about the reaction mechanism: The OTC synthesis mechanism of (4S,6S)-4,6-diphenyl-1,3,5-triazinane-2-thione is initiated with an ammonia benzaldehyde interaction (Scheme 4.2). The interaction of the small substrate molecules
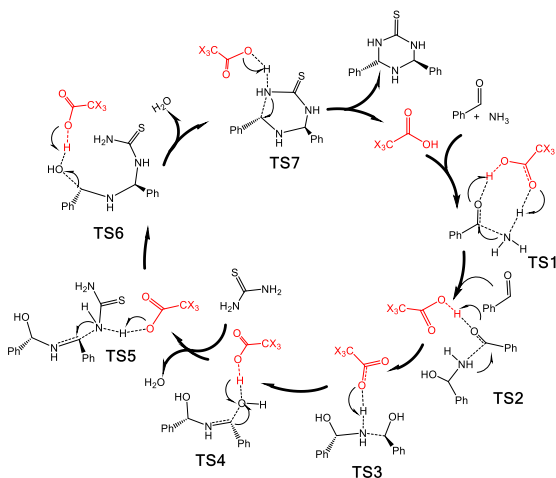
Scheme 4.2. Quantum chemical calculation-based mechanism of CX₃COOH catalyzed OTC condensation reaction.

34

(benzaldehyde and ammonia) is relatively shallow in energy and can be accepted as a starting point in a multicomponent fusion mechanism. The amine group of this intermediate is reacted further with additional benzaldehyde molecule. After the dehydroxilation step (**TS4**) the thiourea amine group attacks to olefinic carbon of the intermediate (see **TS5**). Further dehydroxylation (**TS6**) and proton abstraction (**TS7**) result in the product ((4S,6S)-4,6-diphenyl-1,3,5-triazinane-2-thione) formation. We calculated the reaction (Figure 4.1) cycle three times changing the hydrogen atoms of the methyl group in AA with fluorine and chlorine atoms. The reaction profile diagram in Figure 4.1 includes the three cycles of the OTC mechanism, with the AA, TFA, and TCA catalyst, respectively. The computation shows that there is no large difference in energy barriers (see energy span) in the AA and TFA catalyzed routes (grey and blue in Figure 4.1). Interestingly, TCA minimizes energy barriers considerably compared to AA and TFA.
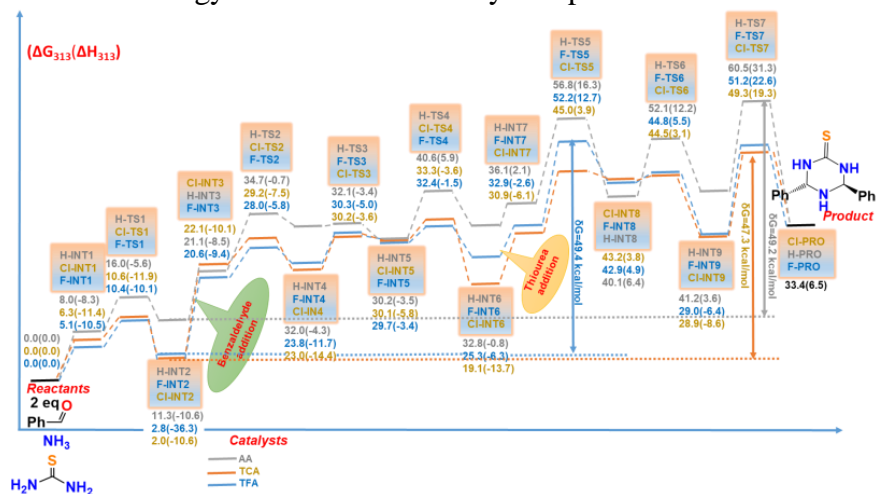
Figure 4.1. Reaction profile (kcal/mol) for the OTC triazinane-2-thione formation according to DFT calculations. Blue, orange and grey colors correspond to the TFA, TCA, and AA catalyzed routes.

Structural analysis of the initial three transition states of Figure 4.2 clearly shows how the halogen atom affect the energy barriers. As seen from the **F-TS1** and **Cl-TS1** the catalyst O-H bonds (1.08Å and 1.10Å) are elongated compared to the AA (1.04Å) case (**H-TS1**).

Replacement of the methyl hydrogen atoms with halogen atoms in AA facilitates proton transfer via the elongated O-H bonds. Proton migration to the oxygen of the benzaldehyde carbonyl can be possible by about 6 kcal/mol lower energy barrier as a result of the bond elongation. The benzaldehyde interaction with azanediylbis(phenylmethanol): **F-INT2, Cl-INT2,** and **H-INT2**) requires higher activation energy (**F-TS2** 25.2 kcal/mol and **Cl-TS2** 27.2 kcal/mol) in the case of halogenated acetic acids for **INT2→TS2**. AA acts as a reasonable catalyst here rendering proton transfer to the carbonyl oxygen via 23.4 kcal/mol energy barrier. AA is also superior catalyst for the dialkylammonium (-NH$_2^+$-, **H-INT4**) deprotonation (**H-TS3**, $\Delta G^{\ddagger}$=0.1 kcal/mol). This can be rationalized with the AA binding to the structure (See Figure 4.2, **H-TS3**) via hydrogen bonding (1.68Å) between the hydroxyl and the AA carbonyl group.
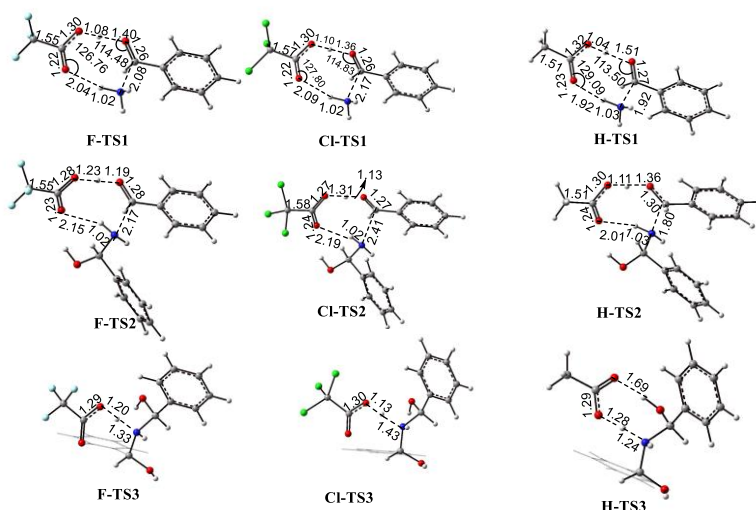
Figure 4.2. The optimized structures of **F-TS1, F-TS2, F-TS3**, **Cl-TS1, Cl-TS2, Cl-TS3, H-TS1, H-TS2** and **H-TS3** with important bond lengths (given in Å), and angles (deg.). Phenyl groups are omitted for clarity.

This kind of behavior is not seen in analogous halogen bearing transition states (**F-TS3** and **Cl-TS3**). In these transition states, the carbonyl of the catalyst and the hydroxyl cannot be prone making a

hydrogen bonding because of the low electron density (electron density flows toward halogen atoms) on the carbonyl oxygen.
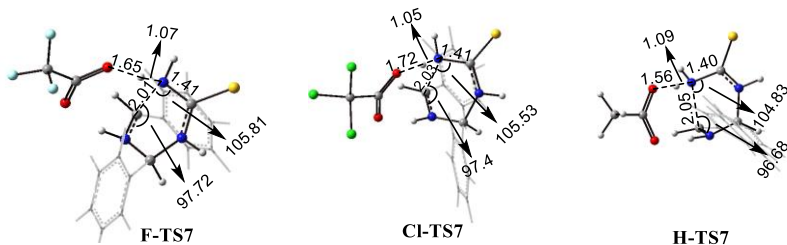

Figure 4.3. The optimized structures of **F-TS7, Cl-TS7,** and **H-TS7** with important bond lengths (given in Å), and angles (deg.). Phenyl groups are omitted for clarity.

TS7 for all three cases (grey, blue, and orange) is a concerted transition state because of proton abstraction from the thiourea amine group with simultaneous ring closure. The activation energies are 22.2 kcal/mol, 19.3 kcal/mol and 20.4 kcal/mol respectively for **F-TS7, H-TS7,** and **Cl-TS7**. The overall reaction is calculated to be 33.4 kcal/mol endergonic reaching the product as a trans conformer.

In ref. , the solvent induced conversion of the cis conformer to trans in a polar solvent, and the stability of the trans conformer, were studied by XRD and NMR analysis. Our calculations are in good agreement with the experimental observation showing the trans conformer ((4S,6S)-4,6-diphenyl-1,3,5-triazinane-2-thione) is stable in the water medium. A cis version of the TS7 could not be established despite several attempts. Moreover, trans arrangement of the product phenyl groups is started from **TS3** and in further optimized transition states and intermediates.

5. Synthesis fluorescent studies of azo-group containing multisubstituted imidazoles

Scheme 5.1. One-pot four-component cyclocondensation reaction
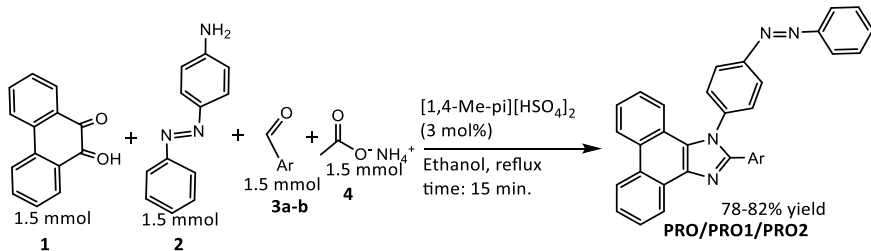
№	Ar	Ar⌒O	Məhsulun adı	Zaman (dəq)	TOF (saat⁻)	Çıxım (%)
1	C$_6$H$_5$-	3a	**PRO**		104	77.6
2	4-MeOC$_6$H$_4$-	3b	**PRO1**	15	109	82.0
3	2,4-Cl$_2$C$_6$H$_3$-	3c	**PRO2**		107	80.3

The IL catalyst ([Me$_2$pi][HSO$_4$]$_2$) is taken for the fusion reaction of Scheme 5.1. Substituents and the product yield, including TOF numbers for each reaction are given in the above table. The incorporation of sulfuric acid to the 1,4-piperazine is confirmed by FT-IR. Stretching wavenumbers (1368, 1456 cm^{-1}) corresponds to S=O in hydrosulfate. The broad signal at 3400 cm^{-1} relates to the HSO$_4^-$ hydroxyl group. The IL structural analysis shows that it can exist in cis and trans form depending on two HSO$_4^-$ ions (anion part) location relative to the cation part (Me2pi) (Figure 5.1).
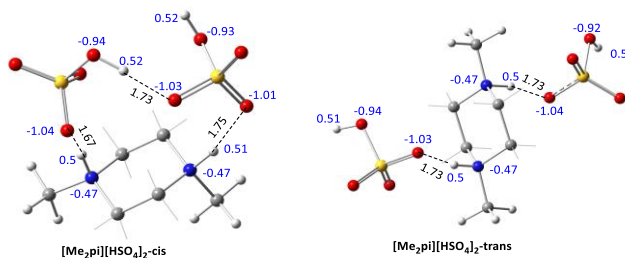

Figure 5.1. The cis and trans conformers of the Me$_2$pi[HSO$_4$]$_2$ IL. Natural charges are given in blue. Bond lengths (black) are described in angstrom (Å). Some hydrogen atoms are omitted for the sake of

clarity. Computational investigations were carried out based on the fusion of the starting compounds: **3a** (benzaldehyde), **1**, **4** (ammonia), and **2**. The Gibbs energy profile (Figure 5.2) proceeds with shallow energy barriers up to **INT5** (diamine) formation. **TS1** is **3a** and ammonia interaction yields **INT1**. Deprotonation of **INT1** yields aminoalcohol (**INT2**), which forms imine (**INT3**) via the dehydration transition state (**TS3**). **INT3** is reacted with **2** forms **INT5**. **INT6** is the addition of **1** to **INT5**, and its conversion to **INT7** is calculated to have the highest barrier (26.56 kcal/mol), which can be considered as a rate-limiting step.
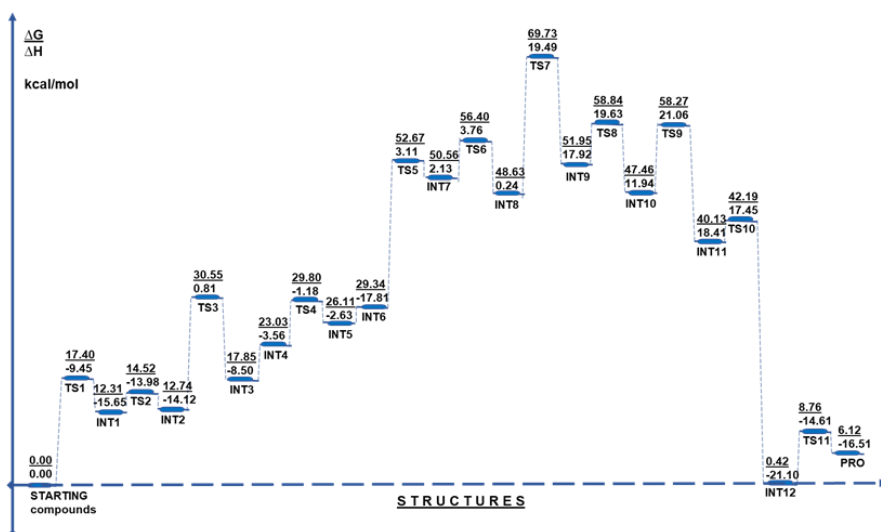
Figure 5.2. Gibbs energy profile of the IL (Me$_2$pi][HSO$_4$]$_2$) catalyzed cyclocondensation reaction (Scheme 5.1). Formation Gibbs energies and enthalpies of the structures are given as ΔG/ΔH kcal/mol.

Further stages are quite straightforward to reach the product. **INT7->INT8** transformation is calculated to have 5.8 kcal/mol energy barrier. It follows the crucial hydroxyl removal (dehydration) step with 21.1 kcal/mol barrier. The final carbonyl group (originally located at **1**) is protonated, and the amine group attacks to the carbon occur simultaneously resulted in the ring closure, which is demonstrated as a concerted transition state (**TS8**) with smaller (6.9 kcal/mol) barrier

(Figure 5.3).

The protonated carbonyl is converted to hydroxyl group then further protonation (**TS9**, 10.81 kcal/mol) renders water extrusion from the structure. Interestingly, the $C(sp^3)$-H activation barrier (**TS10**, 2.06 kcal/mol) is calculated to have shallow energy with the utilized IL catalyst.
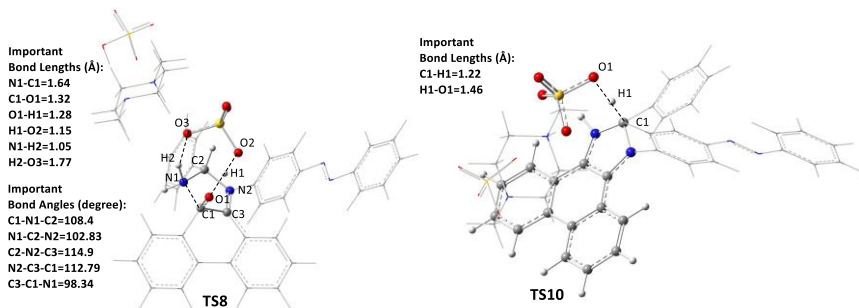

Important Bond Lengths (Å):
N1-C1=1.64
C1-O1=1.32
O1-H1=1.28
H1-O2=1.15
N1-H2=1.05
H2-O3=1.77

Important Bond Angles (degree):
C1-N1-C2=108.4
N1-C2-N2=102.83
C2-N2-C3=114.9
N2-C3-C1=112.79
C3-C1-N1=98.34

TS8

Important Bond Lengths (Å):
C1-H1=1.22
H1-O1=1.46

TS10

Figure 5.3. Optimized structures of the ring closure (**TS8**) and the $C(sp^3)$-H activation (**TS10**) transition states. The cation part of the IL and the aromatic rings are omitted for clarity.

A similar $C(sp^3)$-H activation barrier was calculated a little higher with a different IL catalyst previously. The lower barriers may be the result of the structure conversion to the annulated from (**INT11**) and the strong acidity of the catalyst. The final proton removal transition state (**TS11**) activation energy is 8.34 kcal/mol for converting **INT12** to the final product (**PRO**). The overall reaction Gibbs free energy ($\Delta_r G$) is calculated 6.12 kcal endergonic. The structural analysis of the ring closure (**TS8**) transition state (Figure 5.3) shows that carbonyl protonation occurs via elongation of H1-O2 bond to 1.15 Å while the ring is closing via nucleophilic attack of the nitrogen (N1) to the carbonyl carbon (C1) with 1.64 Å bond length. $C(sp^3)$-H activation (**TS10**) optimized bond distance is 1.22 Å, which follows proton (H1) transformation to the IL O1 via 1.46 Å. The calculated mechanism of the reaction (Scheme 5.2) is started with **3a** and ammonia interaction, which was scrutinized in the previous work. Because of the superior catalytic performance of the IL, the incorporation of the weak nucleophile (**2**, aromatic amine) to the imidazole structure (**PRO**)

became possible.
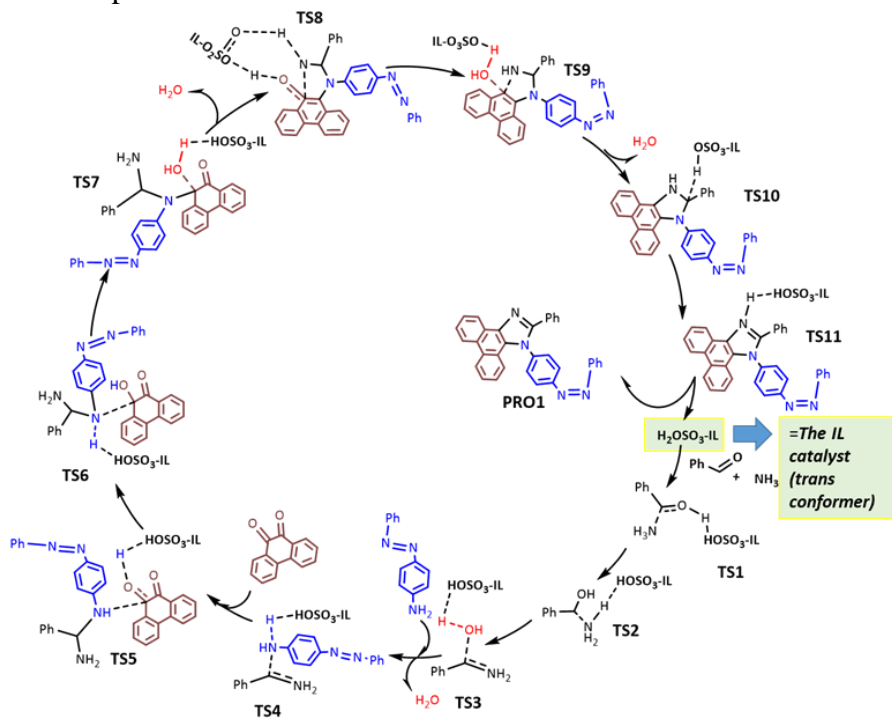
Scheme 5.2. Calculated mechanism of the reaction. Intermediate structures are not given to avoid clutter.

6. Vegetable oil epoxidation, aminolysis, and related computational mechanistic studies.

For the present mechanistic studies, we chose a model reaction to reduce computational time: Instead of macromolecular triglyceride, but-2-ene was taken as the double bond carrier. Since the macromolecular triglycerides have very flexible structures, we do not expect the reaction pathways to be influenced strongly by steric bulk. Hydrogen peroxide (H_2O_2, **HP**), peracetic acid (CH_3CO_3H, **PA**), and performic acid (HCO_3H, **PF**) were utilized as oxidizing agents. For the nucleophilic epoxide ring-opening, Lewis acidic catalysts ($ZnCl_2$, $NiCl_2$, and $FeCl_2$) and ethylamine (nucleophile) were examined.
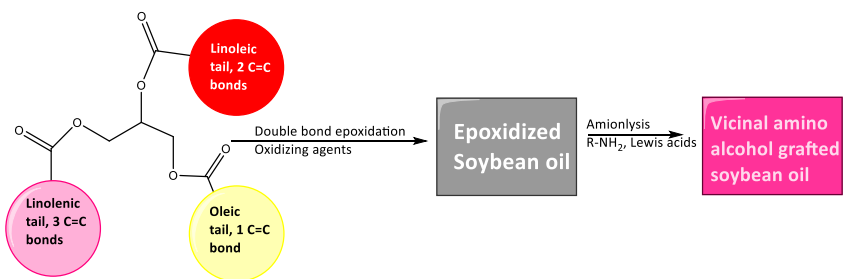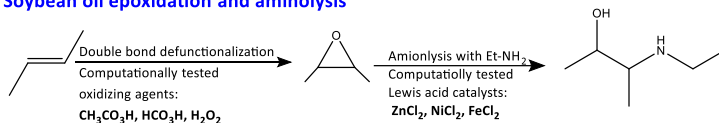
Scheme 6.1. The unsaturated fatty acids triglyceride conversion to the lubricant precursors.

Mechanistic studies. Effective epoxidation of vegetable oils is one of the challenging processes, which determines the efficiency of the next step treatment, i.e., hydroxylation, N-alkylation, O-alkylation. Figure 6.1 shows **HP**, **PA**, and **PF** mediated epoxidation routes. Effective epoxidation of vegetable oils is one of the challenging processes, which determines the efficiency of the next step treatment, i.e., hydroxylation, N-alkylation, O-alkylation. Figure 6.1 shows **HP**, **PA**, and **PF** mediated epoxidation routes. **HP** was employed previously as an oxidizing agent in vegetable oil epoxidation processes. The computations show that **HP** is not an effective oxidizing agent for the epoxidation, due to the high energy barrier (39 kcal/mol). In comparison, the **PA** and **PF** activation energies are 9.2 kcal/mol and 12.3 kcal/mol lower, respectively. Since **PF** gave the reaction with the lowest barrier (26.7 kcal/mol) the reaction was recalculated, including the solvation model for n-hexane. Investigations show that the **PF** route activation energy is decreased by 4 kcal/mol compared to the gas-phase condition.
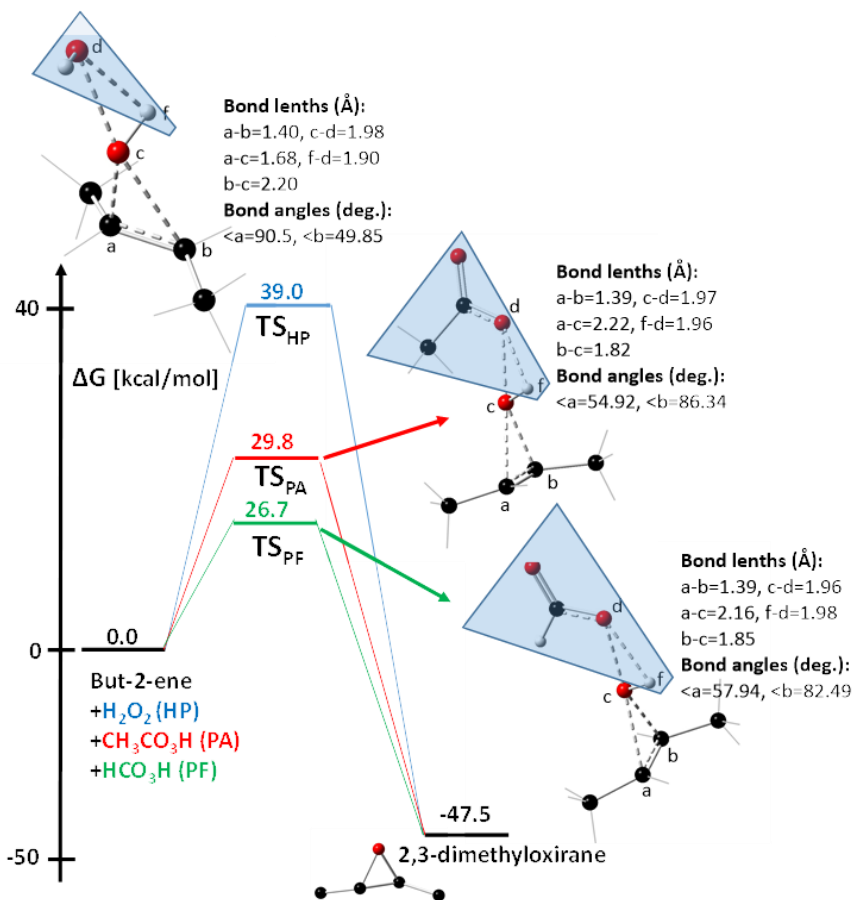
Figure 6.1. Free energy profile for the epoxidation of but-2-ene. Blue, red, and green colors correspond to the **HP**, **PA**, and **PF** employed routes. In the TS structures the but-2-ene hydrogens are omitted to avoid clutter. The blue shaded areas indicate leaving molecules (H_2O, HCOOH, and CH_3COOH) after oxidation.

We focus here on the gas-phase reaction profiles, because of experimentally employed solvent-free epoxidation conditions for the unsaturated fatty acid esters.

The epoxide ring-opening was initially calculated in a catalyst-free condition (Figure 6.2):
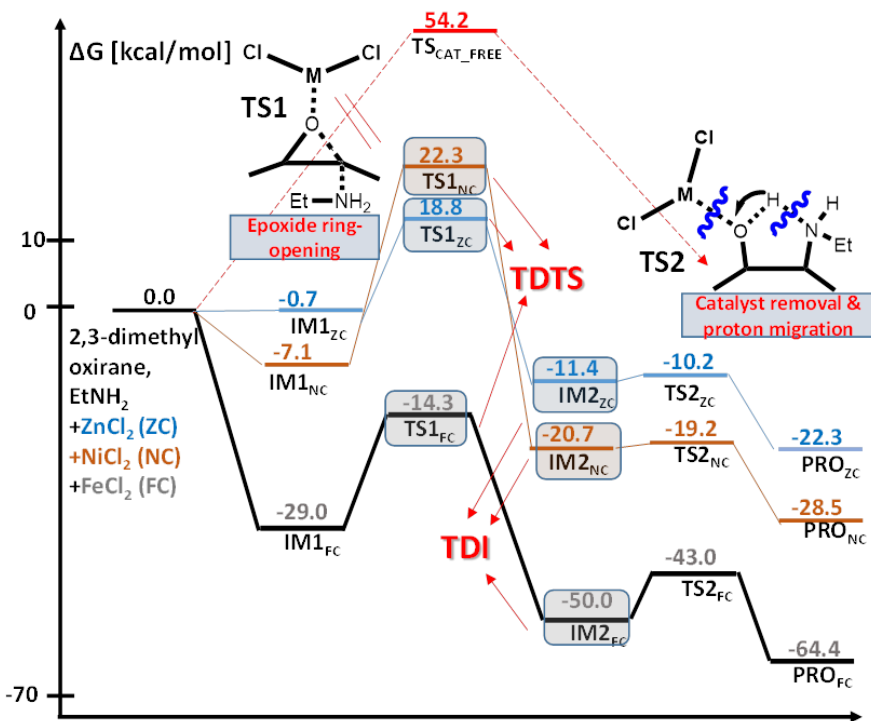
Figure 6.2. Gibbs energy profile for the oxirane ring opening in the catalyst-free and catalytic conditions. Red: catalyst-free, blue: ZnCl$_2$, orange: NiCl$_2$, grey: FeCl$_2$ promoted catalytic routes. Singlet spin state Gibbs energies are reported for the ZC and NC catalytic cycles. Since triplet spin state is determined as a ground state related Gibbs energies are included to the energy profile.

Concerted **TS$_{CAT\_FREE}$** is obtained for the one-step direct transformation of EtNH$_2$ and 2,3-methyloxirane to 3-(ethylamino)butan-2-ol (**PRO**) via 54.2 kcal/mol energy barrier. A similar energy barrier was calculated previously for the epoxide ring-opening in catalyst-free condition. The calculated energy barrier shows that utilizing a catalyst will be a cost-effective option for the process. Because of the extensive application of Lewis acid catalysis in the aminolysis of epoxides to β-amino alcohols, we chose ZnCl$_2$, NiCl$_2$, and FeCl$_2$ for the calculations. In particular, aminolysis of the

44

epoxidized unsaturated fatty esters has been carried out with $ZnCl_2$. As seen from Figure 6.2, the Lewis acid coordination and Et_2NH_2 nucleophilic attack go through a concerted TS (**TS1**). It can be considered the rate-limiting step for all three reaction routes (ZC, NC, FC). In the case of the $ZnCl_2$ catalyzed cycle, the ring-opening energy barrier is calculated to be 19.5 kcal/mol (relative to **IM1zc**). The analogous barrier is found to be 14.1 kcal/mol and 14.7 kcal/mol for the $NiCl_2$ and $FeCl_2$ routes, respectively. We recalculated FC including solvent effects (solvent: n-Hexane) and observed only small changes (less than 3 kcal) in the energy barriers.

7. Computational mechanistic studies of 5-HMF synthesis from glucose

We tested various catalytic systems on the glucose dehydration reaction. Based on the above in-depth investigations, we chose [DPhDA]HSO4 as a superior catalyst for efficient glucose dehydration to 5-HMF. The reaction was carried out at the 100-160 oC temperature range with 30 mol% catalyst loading in 15-180 minutes time range. As seen from the figure, increasing reaction time up to 120 min positively affects the 5-HMF yield in the case reactions carried out at 100-140 °C. The yield slowly goes down beyond 30 min if we heat the reaction mixture to 160 °C. The maximum achievable 5-HMF yield is observed to be 78% at 100 °C in 120 min while the reaction at 120 °C reaches the maximum 5-HMF yield (73.4%) in 90 min. The best reaction condition can be suggested in 30 min at 160 °C and 120 min at 140 °C, which resulted in quantitative 5-HMF yields, 91.4%, and 94.0%, respectively. To display the effectiveness of IL [DPhDA]HSO4 catalyst, we conducted a recycle test via carrying out five runs of the experiment, each with a 30 min reaction time at 160 °C. After each run, 5-HMF was extracted with diethyl ether carefully, and then the remaining residue was controlled with UV-vis analysis to ensure the vanishing 5-HMF and glucose signals. Fresh glucose was added to the catalyst/DMSO mixture for the next run. IL catalyst can be utilized for the three consecutive runs without a significant decrease in 5-HMF yield. We chose α-glucose as the starting compound for the mechanistic studies since its formation Gibbs energy is 4 kcal lower

than for β-glucose and 14.6 kcal lower than for the open-chain glucose (**I1**) conformers. As seen from the energy profile (Figure 6.1), α-glucose ring-opening (**TS1**) occurs via a 20.4 kcal/mol barrier.
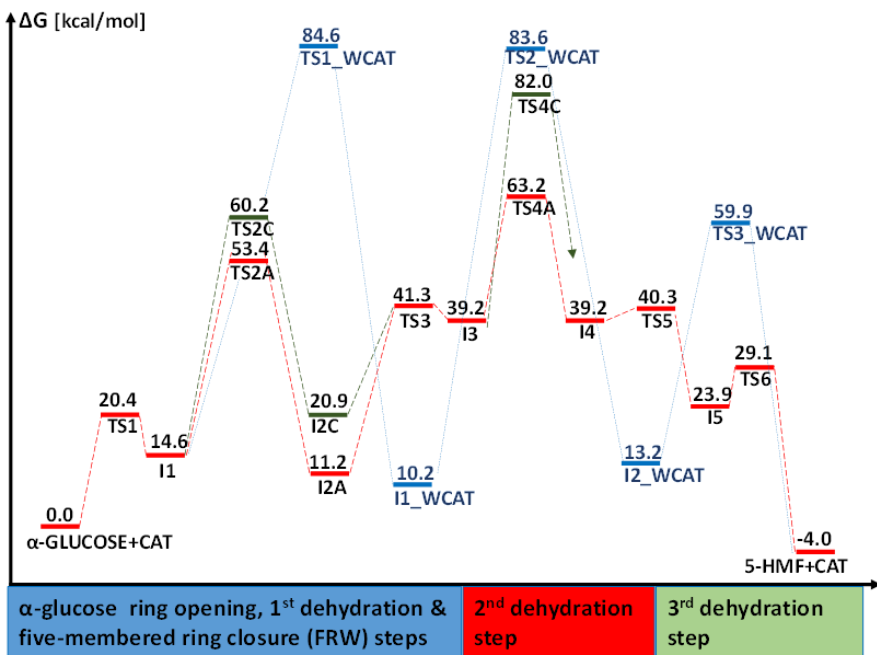

Figure 7.1 Gibbs energy profile of the IL (DPhDA]HSO$_4$, **CAT**) catalyzed α-glucose conversion to 5-HMF. TSs and intermediate names contain **WCAT** (without catalyst), which shows passive incorporation of the catalyst to the species in blue route.

In most previous mechanistic studies , it was suggested that α-glucose is isomerized to the open-chain conformer and then re-isomerized to fructose, which is dehydrated to 2,5-anhydromannose (**I2A** or **I2C**) as a three-step process. Marullo *et al.* transformed glucose to fructose (ca. 50% yield) and then performed the second experiment for the fructose dehydration to 5-HMF . This study did not consider the possibility of the direct conversion of glucose to dehydrated fructose (**I2A**, Scheme 7.1).
.

46
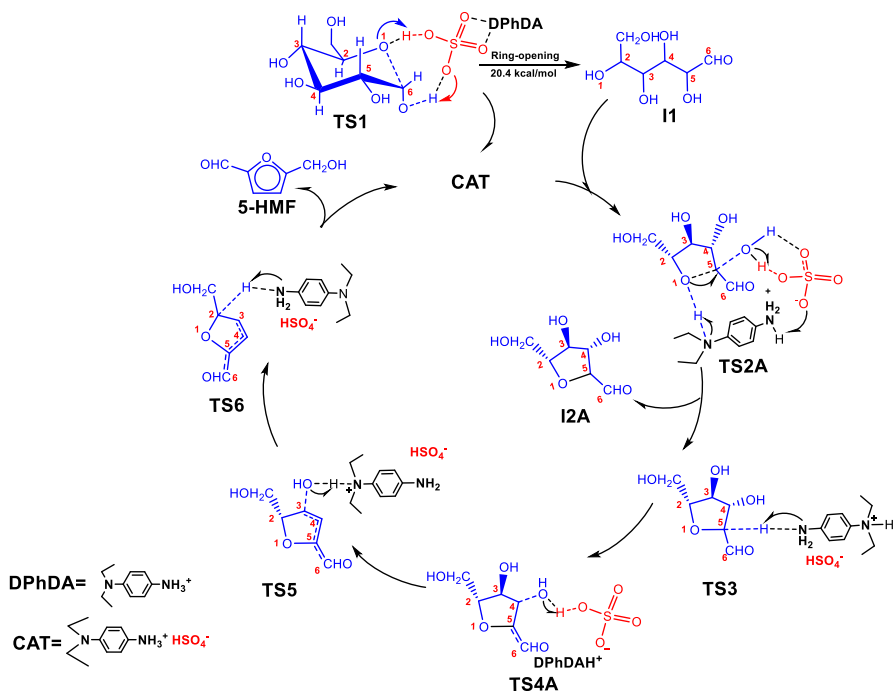
Scheme 7.1. Calculated mechanism of the α-glucose dehydration to 5-HMF. Some intermediate structures are not shown for the sake of clarity.

The basic part of the IL plays the same role as a proton abstractor, but the acidic end is replaced with HSO_4^- in **TS2A**. The IL cation and anion components synchronized effects resulted in an even smaller barrier (38,8 kcal/mol, red route in Figure 7.1) relative to the **TS2C** and **TS1_WCAT** for the FRW step. Based on the investigations mentioned above, we propose the red route as the best catalytic option for the rate-controlling FRW. The second dehydration step is observed to be 24 kcal/mol with the IL anion component proton donation (**TS4A**). The same step is possible with the IL cation component support via relatively high energy (**TS4C**, 42.8 kcal/mol). **TS2_WCAT** is also responsible for the catalyst-free concerted second dehydration and deprotonation step through a very high barrier (73.4 kcal/mol) relative to **I1_WCAT**.

8. Computational mechanistic studies on the poly-p-phenylenediamine formation.

The conversion of p-PDA into free-radical is required to initiate the polymerization reaction. Experimentally it was carried out by mixing the monomer and $K_2S_2O_8$ in aqueous media. So, we initially decided to consider the possible interaction of water molecules on the persulfate precursor. We start the computation to observe the mutual role of $S_2O_8^{2-}$ and water on the p-PDA transition to free-radical. Therefore, the free-radical formation step of p-PDA was simulated with $S_2O_8^{2-}+2H_2O$ (**TS+2H₂O**) and $S_2O_8^{2-}+H_2O$ (**TS+H₂O**) clusters to show the energy barriers. Two water molecules are incorporated into $S_2O_8^{2-}$; one is taking part in direct deprotonation of the p-PDA amine group

A small reduction (6.7 kcal) in the energy barrier with almost no changes in the bond lengths in **TS+H₂O** show that additional water molecules serve as a solvation medium. Alternatively, a TS for the persulfate sulfur atom direct incorporation for the p-PDA conversion to free-radical via removing the p-PDA amine group proton was successfully located. A similar high energy barrier was obtained for (**TS-S**) 51.7 kcal/mol, which directed us to focus on the SFR, PA, and PP routes. Because of the previous suggestion about possible decomposition probabilities of persulfate ion in aqueous media, the p-PDA dimerization is calculated trice with SFR, PA, and PP.

The free-radical formation TS (**TS1K**, $\Delta G^{\ddagger}=-37.7$) is calculated to have the lowest energy compared to the SRF and PA routes. Şəkil
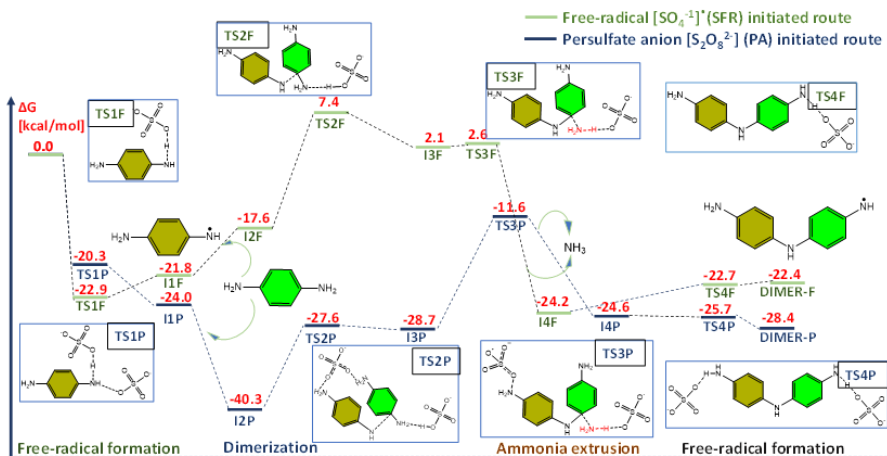
Figure 8.1 Reaction profile for p-PDA dimerization: SFR initiated route (green), PA initiated route (blue).

Considering the decomposition probability of sulfate dimer (persulfate) into two SFR the dimerization cycle of p-PDA was first calculated with SFR (Figure 8.1, blue route). As seen from the reaction profile (RP), the energy of the pre-reaction complex is not described before **TS1F** since p-PDA conversion to free-radical is a barrierless process The free-radical attack on the second monomer is calculated to have the highest barrier (29.2 kcal/mol).

9. The optimization of cyanuric acid synthesis from urea pyrolysis and related mechanistic studies

The yield investigation of the urea pyrolysis to **CA** was performed based on five variables: type of ILs, catalyst (IL) loading, reaction temperature, reaction time, and solvents. The highest yield ($68 \pm 2\%$) of **CA** was observed in the neat conditions in the presence of [dmaH][HSO$_4$], (IL : Urea; 5:1, w:w) at 220 °C for 25-30 minutes. Solvents with high boiling points, i.e., naphthalene, nitrobenzene, ethylene glycol, and DMSO were tested on the reaction with constant solvent and IL ratio (1:1, w:w) to investigate the impact of solvent on the reaction yield. The solvent utilization does not contribute to the

CA yield in all cases. Temperature optimizations showed that The CA yield increases with increasing temperature up to 220 °C, and beyond this point, CA formation declines significantly. The IL [dmaH][HSO₄] recycle test over five cycles was performed for the urea pyrolysis reaction (IL : Urea; 5:1, w:w) at 220 °C for 30 min period. The catalyst preserves its effectiveness for four cycles.

We first calculated the IL-free route to see a clear picture of the IL role in the urea pyrolysis to **CA**. As seen in (green route), 61.9 kcal/mol energy is required to overcome the barrier (**TS1F**) for biuret (**I1F**) formation via ammonia extrusion. The addition of the next urea results in the formation of triuret (**I3F**), via a 59.2 kcal/mol (**TS2F**) energy barrier. Final cyclization of triuret (**TS3F**, $\Delta G^{\ddagger}=52.6$ kcal/mol) yields **CA**.
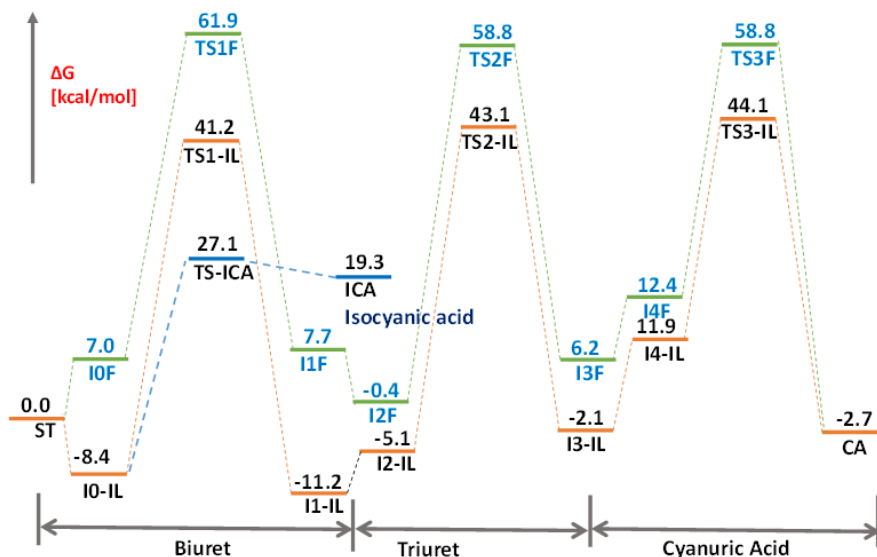

Figure 9.1 Energy profile for the urea pyrolysis to CA: IL-free route (green), IL-mediated urea conversion to CA (orange), IL-mediated ICA formation from urea (blue).

Ammonia extrusion is very critical in each step to maintain urea dimerization, trimerization, and eventually **CA** formation. As seen from the concerted **TS1-IL** structure (Scheme 9.1), one of the urea -

NH₂ (**N2**) groups accept a proton from IL (**N2**-**H2**: 1.05 Å), and the **C-N2** bond elongated up to 1.65 Å, which facilitates nucleophilic attack of the next urea (**N1**) to the electrophilic carbon (**C**) via 1.67 Å bond length. Eventually, simultaneous proton donation and acceptance from IL results in NH₃ extrusion; this scenario is replicated in the next two steps as **TS2-IL** and **TS3-IL**, yielding **CA**. The calculated mechanism of the IL-mediated urea pyrolysis is shown in Scheme 9.1, to understand better the IL role in the **CA** formation.
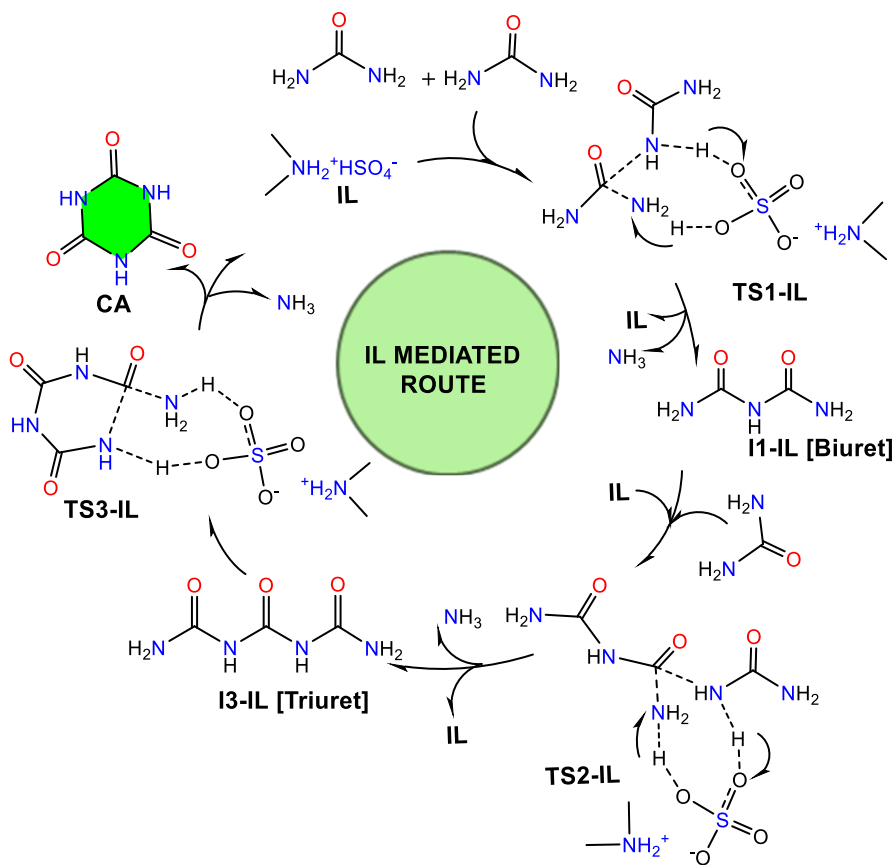
Scheme 9.1 The calculated mechanistic cycle of the IL-mediated urea pyrolysis to CA (Figure 9.1, orange route).

The ammonia extrusion in the first stage, which result in biuret formation is repeated up to triuret stage then its cyclization is quite straightforward process to yield full aromatic cyanuric acid scaffold. As seen in Figure 9.1, the dimerization of urea is higher in energy than isocyanic acid formation. The fact supports more reasonable lower in energy trimerization of isocyanic acid to cyanuric acid. Isocyanic acid trimerization was tested in the IL-free and IL-included versions. As depicted in Figure 9.2 IL catalytic (IL-included) path energy barriers are shallow compared to IL-free route.
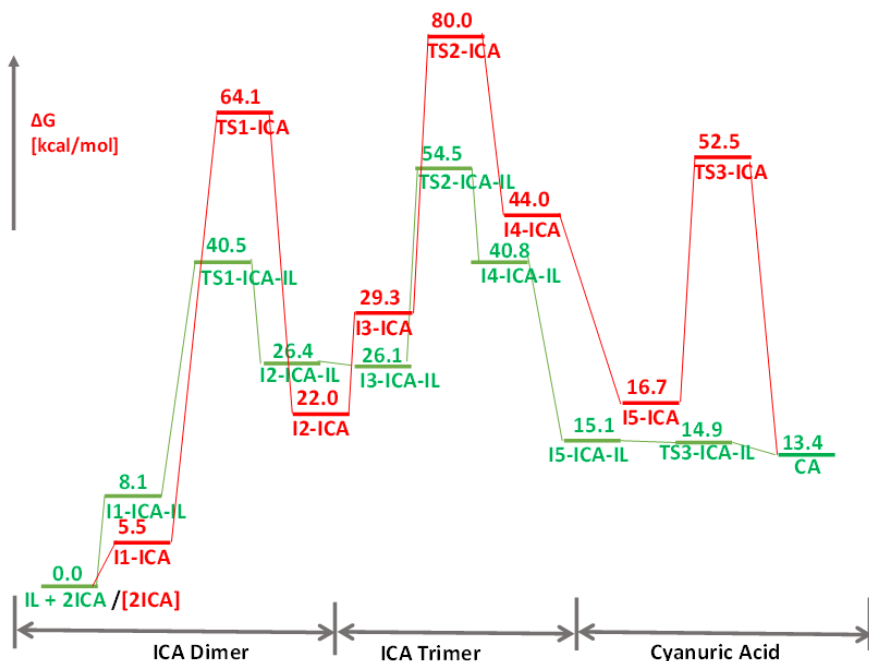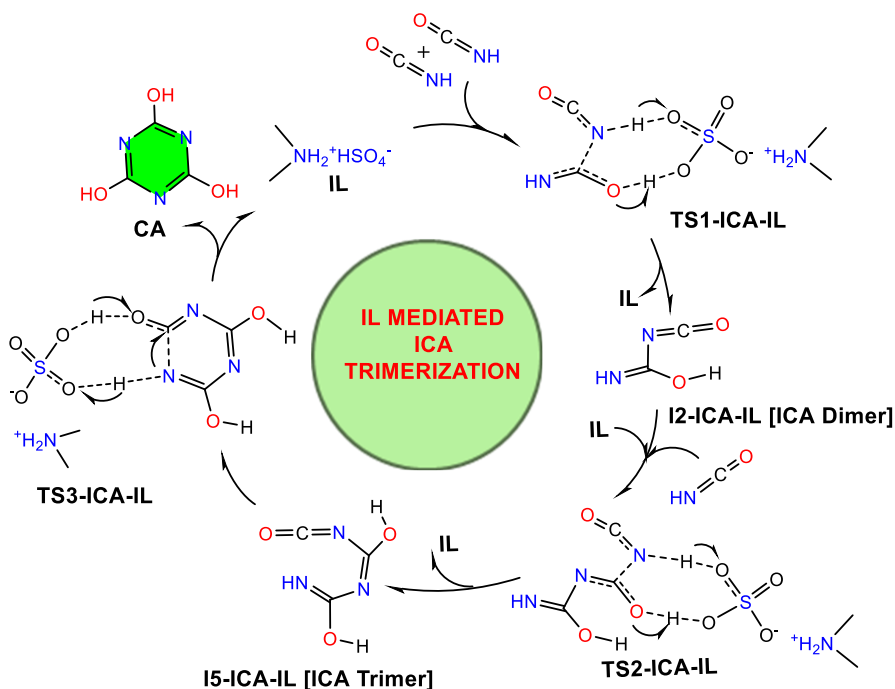

Figure 9.2. Energy profile for the ICA trimerization to CA: IL free route (red), IL mediated (green).

DFT calculations were proposed IL mediated mechanism according to the following scheme (Scheme 9.2).

Scheme 9.2. The calculated mechanistic cycle of the IL-mediated ICA trimerization to CA (Figure 9.2, green route).

10. **Mechanistic DFT studies on carbon dioxide conversion to five-membered heterocyclic organic compounds.**

Extensive emissions of CO_2 due to anthropogenic factors resulted in rising CO_2 levels in the atmosphere, which causes adverse climate change (e.g., temperature rise, sea-level elevation, and wildfires). Therefore, it is very urgent to tackle the CO_2 emission. Scientists have done intensive research on CO_2 sequestration so far. Ethylenediamine (EDA) and its derivatives were used as a substrate for CO_2 conversion in the presence of highly toxic metal catalysis. The conditions of the studied reactions need improvement via a 'green' approach: A low-cost and non-toxic catalyst development is vital for CC because of the environmental concerns. Because of the aforementioned reason, CO_2 fixation with various substrates were considered in the presence of the

ionic liquid catalysis.

The CB step is calculated to have a 1.4 kcal/mol energy barrier (**TS1$_{EDA}$**) to form **I2$_{EDA}$** ((2-aminoethyl)carbamic acid). The IL-mediated RCD of **I2$_{EDA}$** is going through a high energy barrier (**TS2$_{EDA}$**, $\Delta G^{\ddagger}$=32.8 kcal/mol) to reach **P$_{EDA}$** (imidazolidin-2-one) (Figure 10.1).
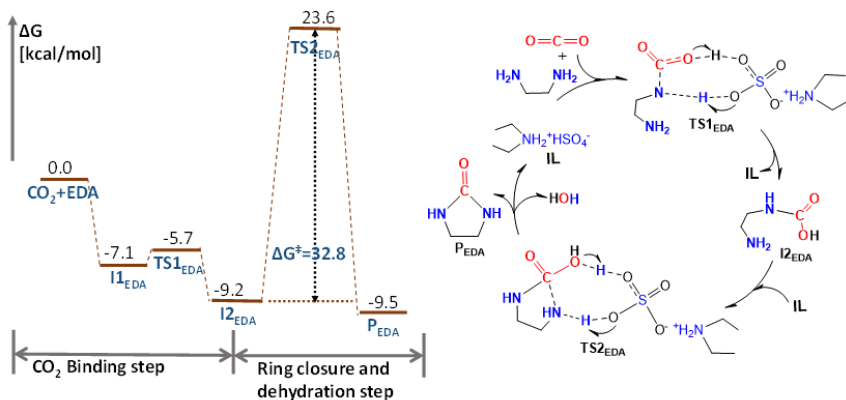

Figure 10.1. Free energy profile (left) and related calculated mechanism (right) of the IL (Et$_2$NH$_2$]HSO$_4$ catalyzed CO$_2$ conversion to imidazolidin-2-one (**P$_{EDA}$**).

Exploiting this scenario (Figure 10.1), we added different substituents to EDA, viz., -OH, -N(CH$_3$)$_2$, and -NO$_2$ to assess substituent effects on the CB and RCD energy barriers.
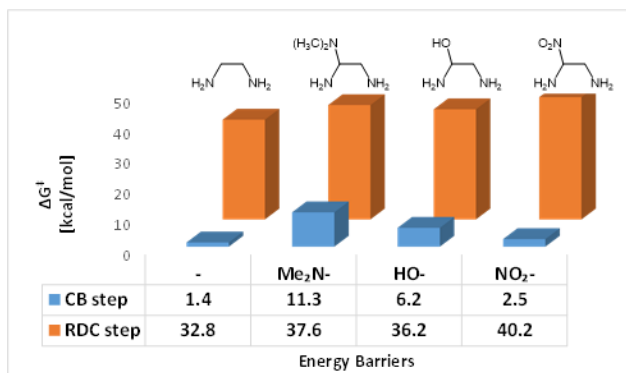

	-	Me$_2$N-	HO-	NO$_2$-
CB step	1.4	11.3	6.2	2.5
RDC step	32.8	37.6	36.2	40.2

Energy Barriers

Figure 10.2. Energy barriers for CB and RCD steps for the EDA derivatives (-OH, -N(CH$_3$)$_2$, and -NO$_2$).

It was identified that addition of various substituents to EDA does not change the energy barriers considerably because of steric hindrance of the used substituents. After the analysis of the EDA-based CO$_2$ fixation, we considered various substrates (ETA, EG, MEA, and EDT) on CO$_2$ fixation computationally since the substrates were utilized extensively in experimental studies
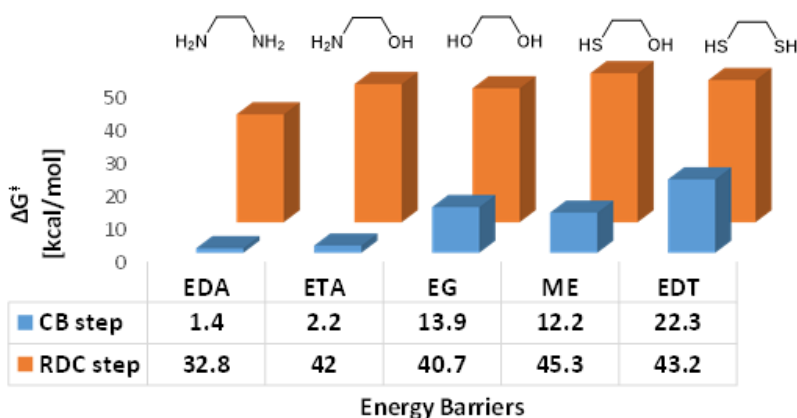

Energy Barriers	EDA	ETA	EG	ME	EDT
CB step	1.4	2.2	13.9	12.2	22.3
RDC step	32.8	42	40.7	45.3	43.2

Figure 10.3. Energy barriers for CO$_2$ binding and RCD steps for the various substrates (EDA, ETA, EG, ME, and EDT) +CO$_2$ cyclization to HCD (1 atm, 298.15 K).

Based on the calculated energy barriers, EDA was identified as the model substrate for fixating CO$_2$ (Figure 10.3). So further optimizations were conducted with only using EDA+CO$_2$ interactions. We tested various solvents via SCRF solvation model on the EDA cycle because of its shallow energy profile. Methanol, THF, acetonitrile, and n-hexane were examined because of their frequent utilization as a solvent in experimental studies related to CO$_2$ fixation. Solvent polarity is one of the important factors influencing the RCD step. Increasing polarity does not affect significantly (ca. ±1 kcal relative to n-hexane) on the CB step (**TS1$_{EDT}$**).

11. Computational approach to counterion-coupled gemini surfactants based on amino alcohol head groups

Computational studies on gemini surfactants with mono- and di-(2-hydroxypropyl)ammonium head-groups: We turn to computation for rationalizing the reaction mechanism and experimentally observed higher conversion of the reactants for both epoxide opening and salt formation routes. Reactions mentioned in Scheme 11.1 are taken for calculations. Scheme 11.1 shows both epoxide opening and salt formation paths.
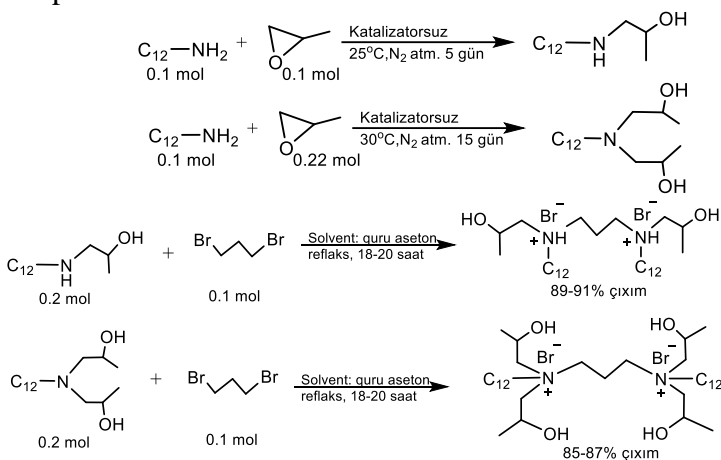
Scheme 11.1. Reaction scheme of the synthesis of mono- and di-(2-hydroxypropyldodecylamines) and synthesis of gemini surfactants based on dibromoalkanes (C3).

Dodecylamine and PO interaction is calculated to have a high barrier (54.2 kcal/mol) and yields mono-(2-hydroxypropyl)dodecylamine (**INT2**).
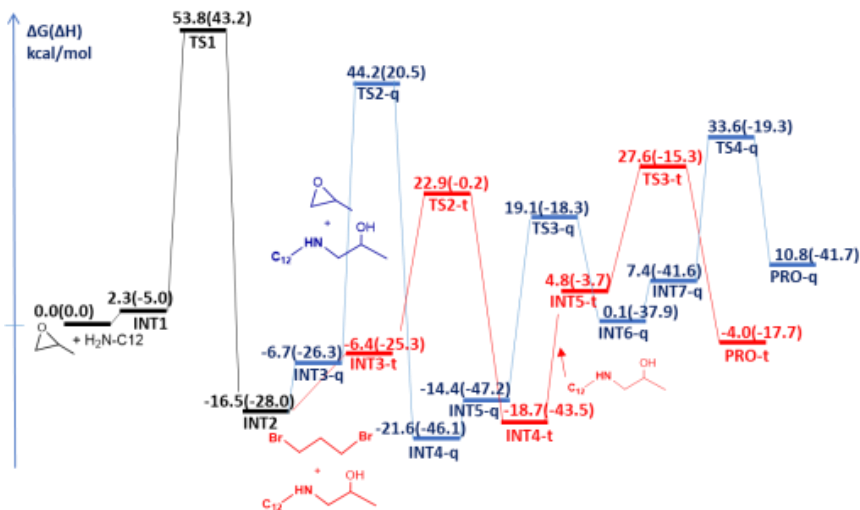
Figure 11.1. Reaction profile for the formation of tertiary (**PRO-t**=C12-3-C12[iso-PrOH]) and quaternary (**PRO-q**=C12-3-C12[iso-PrOH]$_2$) gemini surfactants.

Further reaction profile is divided into two routes: **INT2**+**PO** (blue) and **INT2 + Br-(CH$_2$)$_3$-Br** (red) interactions. According to the blue route, activation energy for di-(2-hydroxypropyl)dodecylamine (**INT4-q**) formation is calculated 4.9 kcal higher in energy than **INT2** formation. It clearly shows conversion of dodecylamine into secondary amine (**INT2**) via epoxide opening makes a little difficulty (steric hindrance) as a nucleophile attacking to the second PO molecule. Direct salt (**INT4-t**) formation (**INT2 + Br-(CH$_2$)$_3$-Br**) activation energy is 41.7 kcal/mol which is not much different than tertiary amine (**INT4-q + Br-(CH$_2$)$_3$-Br**) conversion to salt in activation energy (43.7 kcal/mol). This fact supports experimental observation in regard to the same yield of tertiary and quaternary gemini surfactants . Overall quaternary salt (**PRO-q**) formation reaction is 22.8 kcal/mol (endergonic), whereas tertiary salt (**PRO-t**) formation is 2.2 kcal/mol (endergonic). Optimized structures of the final products are described in Figure 11.2.
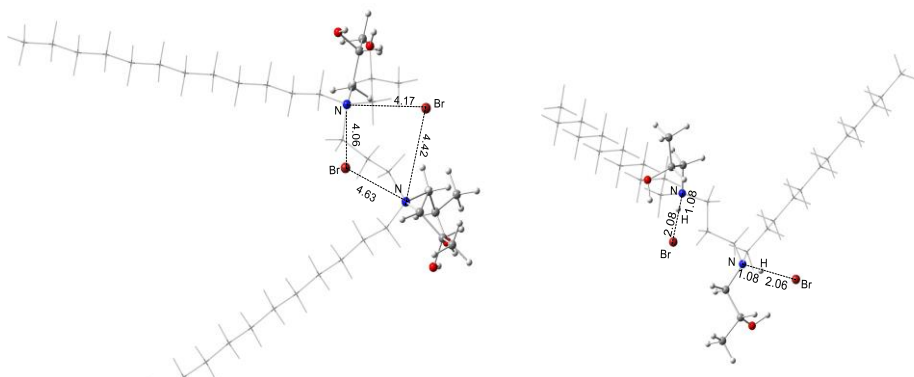
Figure 11.2. Optimized structures with important bond lengths (Å) of
PRO-q (left), **PRO-t** (right). Carbon chains are omitted for clarity.

As seen from the **PRO-q** structure, the closest Br^- and N^+
(quaternary) electrostatic interaction distance is 4.06 Å. Br^- ions are
located closer to the tertiary NH^+ at the **PRO-t** structure: Electrostatic
interaction becomes possible via the middle H atom (N-H-Br) with
bond lengths 1.08 and 2.06 Å.

The epoxide opening (**TS1**) and salt formation (**TS3-q**) transition state
structures are shown in Figure 11.3.

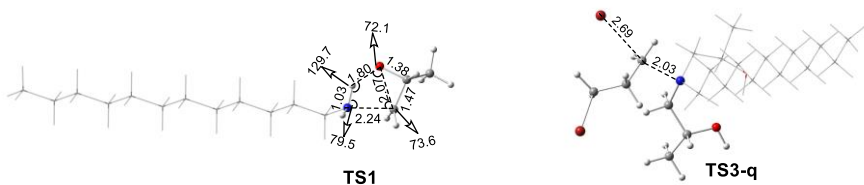**Figure 11.3.** Optimized structures with important bond lengths (Å) of
PRO-q (left), **PRO-t** (right). Carbon chains are omitted for clarity.

As seen in the **TS1** structure, nucleophilic attack of
dodecylamine to an external PO carbon atom is possible via 2.24 Å
bond length. At the same time, the external epoxide ring C-O bond is
elongated to 2.07 Å and the amine hydrogen is attracted by the PO

oxygen with 1.80 Å distance.

The quaternary salt formation transition state (**TS3-q**) is also described in Figure 11.3. The nucleophilic attack of **INT4-q** to 1,3-dibromopropane (**INT5-q**) occurs via **TS3-q** with 43.7 kcal/mol energy barrier. Bromine extrusion (Br-C) and C-N bond formation distances are calculated as 2.69 and 2.03 Å respectively. Energy barriers of the rate limiting epoxide ring opening steps are bigger. The similar barrier was calculated previously for a catalyst-free reaction

Table 11.1. Calculated Gibbs free energies of the synthesized surfactants.

Name	G_{cis}(hartree)*	G_{trans}(hartree)*	$\Delta G_{(cis\text{-}trans)}$(kcal)
CA	-2092.0073	-2092.0032	-2.54
LA	-2249.1543	-2249.1510	-2.11
MA	-2406.2976	-2406.3011	2.20
PA	-2563.4471	-2563.4446	-1.58
OA	-2718.1717	-2718.1756	2.47
SA	-2720.5933	-2720.5925	-0.52

Sum of electronic and thermal Gibbs free energies from the Gaussian output.

Experimental observation shows that OA bears the highest Γ_{max}, and the lowest A_{min} values. Geometry analysis of OA cis and trans conformers indicates that the OA hydrophobic tails are bended because of the double bond (at cis position) located in the middle of the tails (see Figure 11.4). Electrostatic interaction distances between the tail and head group are calculated for O-H (carboxyl group), N-H (the head group nitrogen and acidic proton) as 1.73 Å (angstrom) and 1.03 Å consequently for OA-cis. Because of the awkward orientation of the tail the OA-trans O-H bond distance elongated up to 1.77 Å.
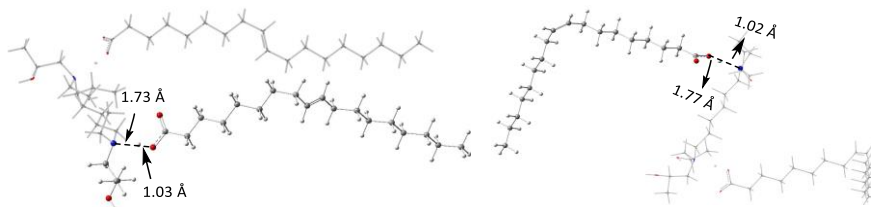
Figure 11.4. Optimized structures of **OA**-**cis**(left) and **OA**-**trans**(right) conformers. Carbon, hydrogen, oxygen, and nitrogen atoms at the tail and head groups are omitted for clarity.
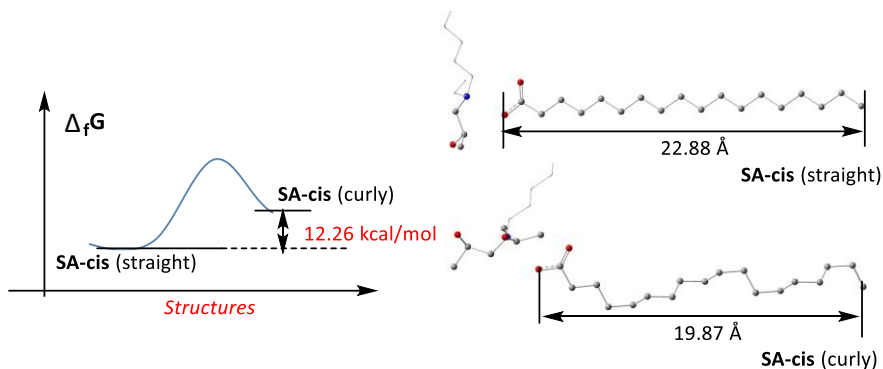

Figure 11.5. Formation Gibbs free energy of the curly conformer. Matching the **SA-cis** conformers tail distances in a straight and curly fashion. Hydrogen, carbon, oxygen, and nitrogen atoms in the structures are omitted for the sake of clarity.

Formation Gibbs free energy of SA-cis curly conformer is calculated to be 12.26 kcal/mol enedergonic. Energy barriers for the single bond rotation were not so high, which is why curling of a long tail may be possible for arriving at a stable micelle with negative formation Gibbs free energy (see Table 11.1) as hypothesized before. As seen in Figure 11.5 curling of the SA-cis resulted in 3.01 nm decrease in the tail length. As described in Table 11.1, OA cis conformer is higher in energy compared to trans. Micellization is more likely with trans conformer which holds even higher space than cis. The obtained geometries are in good agreement with the experimentally observed OA A_{min} value.

Conclusions

1.   **Computational approach to the synthesis of triazepine derivatives.** In conclusion, a practical three-step synthesis for 5H-pyrrolo[2,1-d][1,2,5]triazepine derivatives has been developed starting from pyrrole. The pyrrole derivatives having carbonyl groups at the C-2 position were converted to N-propargyl pyrroles. The

reaction of those compounds with hydrazine monohydrate resulted in the formation of 5H-pyrrolo[2,1-d][1,2,5]triazepine derivatives. Mechanistic studies indicated that the propargyl group first undergoes isomerization to give the corresponding allene which can be trapped by nucleophilic attack of the nitrogen atom of the initially formed hydrazones.[1]

2.   **Computational approach for multicomponent imidazole formation reaction**. The tetrasubstituted imidazole formation reaction was calculated under IL-free, IL-solvation, and IL-catalytic conditions. [2-11] Although IL solvation already leads to a significant lowering of the reaction barriers, the computations show that there are even more effective pathways in which the IL acts as a catalyst via proton transfers. The tetrasubstituted imidazole formation proceeds via intramolecular hydroxylation and deprotonation in the absence of the IL, but the reaction profile affords high barriers. In the presence of the IL, the calculations indicate a number of different interactions. [5,12]

3.   **Computational and experimental approaches for C(sp^3)-H activated imidazole formation.** [5,12] Imidazole and pyrazine rings were synthesized economically via low-cost Brønsted acidic IL catalysts according to "green" requirements. Various imidazoles and pyrazines can be synthesized by the same procedure. Optimization of several conditions were carried out on the benzil and benzylamine cyclization. The reaction reaches a maximum yield of 75% PRO1 and 18% **PRO2** at 90°C and 10 mol% catalyst loading ([deaH][HSO4] IL) in 1 hour. At the optimized temperature (90°C) and catalyst loading (10 mol%), the yield of PRO2 is slightly higher than the yield of PRO1 after 3 hours, and remains constant thereafter, indicating how the reaction reaches its equilibrium.[11]

[Me$_2$pi][HSO$_4$]$_2$ IL catalyzed mutlisubsituted imidazoles were syntheszied in a short period of time (15 min) with good yield (78-82%). Fluroscent properites were deeply analyzed with the TD-DFT support. The reaction mechanism was identified computationally. [17,18]

4.   **Computational approach to triazinane-2-thione synthesis**. Plausible mechanisms were predicted for AA and its halogenated

derivatives to catalyze OTC cyclocondensation to triazinane-2-thione. The product was generated as a trans conformer from the final ring closure transition state. The reaction was calculated to be 33.4 kcal/mol endergonic and experimentally applied temperature (313K) was satisfactory driving force for the product (85%) formation. [13-15] Some sulfo- and rhodanide group containing heterocyclic compounds were synthesized and the reaction mechanism was calculated. [16]

5.   **Computational insights to vegetable oil epoxidation and aminolysis.** The carbon-carbon double bond defunctionalization through epoxidation and the subsequent epoxide ring aminolysis was studied computationally. The H_3CO_3H (PF) energy barrier was found to be smaller ($\Delta G\ddagger=26.7$ kcal/mol, TS1PF) than the other two oxidation routes (Figure 1). The epoxide ring-opening was studied with three Lewis acid catalysts ($ZnCl_2$, $NiCl_2$, and $FeCl_2$). The rate-limiting energy barrier for the FC cycle was found to be 3.4 kcal less than in the ZC cycle. Despite the regular utilization of $ZnCl_2$ in practice, our computations suggest that $FeCl_2$ would be a better catalyst, based on the applied energetic span model. Since iron is an inexpensive metal, we hope that the present calculations will motivate experimental verification of this prediction. We believe this work will contribute to the waste vegetable oils cost-effective industrial utilization. [19]

6.   **Computational and experimental insights to 5-hydroxymethylfurfural synthesis from glucose**. "Greener" and quantitative α-glucose conversion to 5-HMF (91.4% yield at 160 oC in 30 minutes) was carried out in the presence of the low-cost [DPhDA]HSO$_4$ IL. Optimized reaction conditions show that increasing catalyst loading up to 40 mol% was beneficial for the 5-HMF yield elevation at 130 °C in 30 min. Polar aprotic solvents (DMF, DMA, and DMSO) were observed to be better for the α-glucose dehydration reaction compared to nonpolar solvents (dioxane, ethylbenzene). Inspired by the high 5-HMF yield, the IL catalyst structure was studied computationally with the NBO method. [20-23]

7.   **Computational insights to p-phenylenediamine polymerization.** Uncovering the mechanism that results in the

formation of the p-PDA free-radical dimer (DIMER-K) is important to understand the p-PDA polymerization because poly-p-PDA and its modifications have extensive applications in electronic devices. The works focused on the frequently utilized polymerization oxidant/initiator potassium persulfate (PP) role in p-PDA dimerization. The polymerization mechanism was displayed based on the replicated free-radical formation (monomer) → dimerization → ammonia extrusion → free-radical formation (dimer) steps. Since aqueous media was used experimentally, PP dissociation was considered, and the entire cycle was calculated trice: sulfate free-radical (SFR), persulfate anion (PA), and potassium persulfate (PP) cluster mediated routes. [24]

8. **Computational and experimental insights to ionic liquid mediated cyanuric acid synthesis form urea.** The low-cost IL-mediated urea pyrolysis to CA was studied experimentally and computationally. Experimental optimizations based on the time, temperature, solvent, and IL loading showed that ideal urea conversion to CA (~70% yield) was at 220 °C, in 30 min when IL : Urea ratio is 5:1 (w:w). The utilization of cheaper and 'greener' ionic liquid allowed to decrease the CA production cost because previously separate solvent and catalyst were used for the same reaction. The IL's low vapor pressure at 220 °C made it a superior solvent over traditional solvents and allowed it to conduct the reaction in an open flask. Additionally, the IL catalytic activities do not necessitate using a separate catalyst to boost conversion. [25]

9. **Computational predictions about CO_2 conversion to heterocyclic carbonyl derivatives.** CO_2 fixation utilizing various nucleophilic substances was studied. EDA was utilized first in the quantum chemical calculations because of its higher nucleophilicity relative to other tested substrates. The CO2 binding to EDA was calculated to have an effectively barrierless (1.4 kcal/mol) step. The next concerted TS rendered cyclic urea formation via ring closure and dehydration (32.8 kcal/mol). Attaching electron donor and acceptor groups to EDA was found to elevate both CB and RCD steps energy barriers because of steric hindrance issues, therefore it was concluded that unsubstituted substrates are more suitable to fixate CO2 (Figure

66). Theoretical investigations showed that ETA has a similar energy barrier (2.2 kcal/mol) relative to EDA for the CB step since nucleophilic attack was initiated by amine groups in both substrates. [26-28]

10. **Application of quantum chemical calculations to the synthesis of gemini surfactants.** Mono- and di-(2-hydroxypropyl)ammonium head-groups containing surfactants synthesis reaction profile was calculated for the quaternary (PRO-q) and tertiary (PRO-t) gemini surfactants formation. It was identified that PRO-t and PRO-q formation reactions are both endergonic. Epoxide opening reactions via primary (dodecylamine) and secondary (INT2) amines were determined as exergonic via big energy barriers (54.2 and 59.1 kcal/mol). [29-31]

Published references related to the dissertation:

1. Menges N., Sari O., Abdullayev Y., Erdem S.S., Balci M., Design and Synthesis of Pyrrolotriazepine Derivatives: An Experimental and Computational Study // The Journal of Organic Chemistry, 78 -2013 p. 5184-5195.

2. Simpson J., Mohamed S. K., Marzouk A. A., Talybov A. H., Abdelhamid A. A., Abdullayev Y. A., Abbasov V.M., Green synthesis of multi-substituted imidazoles based MEA // 15th Tetrahedron Symposium. Challenging in bioorganic and organic medicinal chemistry, London, UK, -2014.

3. Mohamed S.K., Simpson J, Marzouk A.A., Talybov A.H., Abdelhamid A.A., Abdullayev Y.A., Abbasov V.M., Multicomponent green synthesis, spectroscopic and structural investigation of multi-substituted imidazoles. Part 1 // Zeitschrift für Naturforschung B, 70 -2015, p. 809-817.

4. Abdullayev Y.A, Talybov A.H, Abbasov V.M., Simpson J., Mohamed Sh. K., Marzouk A.A., Abdelhamid A.A, Valiyev I.A, Mamedkhanova S.M., Synthesis of imidazoles on the basis of aminoethanol by using diethylammmonium hydrogen sulfate as a solvent-free catalyst // PPOR, 16 -2015, p. 215-221.

5. Abdullayev Y., Abbasov V, Ducati L.C., Talybov A., Autschbach J., Ionic Liquid Solvation versus Catalysis: Computational Insight from a Multisubstituted Imidazole Synthesis in $[Et_2NH_2][HSO_4]$, // ChemistryOpen, 5 -2016, p. 460-469.

6. Abbasov V.M, Abdullayev Y. A., Ducati L.C., Talybov A.H., Autschbach J., Computational insight to $[Et_2NH_2][HSO_4]$ ionic liquid catalyzed multisubstituted imidazole synthesis // PPOR 17 -2016, p. 169-181.

7. Мамедбейли Э.Г., Талыбов А.Г., Абдуллаев Ю., Новые тетразамещенные имидазолы;синтез и антимикроб-ная активность // Тезисы докладов Кластер конференции по органической химии «Орг Хим-2016» Санкт-Петербург(пос.Репино), -2016, p. 281.

8. Abdullayev Y., Structural analysis of 2-(2,4,5-triphenyl-1h-imidazol-1-yl)ethan-1-ol, Chemical Problems, 4 (2017) 393-396.

9. Abbasov V.M., Abdullayev Y.A., Talybov A.H., Tagizade Z.Y., Kochetkov K.A., Marzouk A.A, Akhmadova S.Z., Synthesis and antimicrobial activity of tetrasubstituted imidazoles // PPOR, 18 - 2017, p. 69-74.

10. Abbasov V.M, Abdullayev Y.A, Talybov A.H, Akhmedova S.Z., Synthesis and antimicrobial activity of allyl containing tetrasubstituted imidazoles // PPOR, 19 -2018, p. 344-349.

11. Valiyev I., Abdullayev Y., Yagubova S., Baybekov S., Salmanov C., Autschbach J., Experimental and computational study of metal-free Brønsted acidic ionic liquid catalyzed benzylic $C(sp^3)$-H bond activation and C-N, C-C cross couplings // Journal of Molecular Liquids, 280 -2019, p. 410-419.

13. Abdullayev Y., Sudjaev A., Autschbach J., Computational investigation of catalytic effects of CX_3COOH $(X = F,Cl,H)$ on the three-component cyclocondensation reaction // Journal of Molecular Modeling, 25 -2019, p. 173.

17. Abdullayev Y., Mammadov A., Karimova N., Talybov A., Yolchuyeva U., Autschbach J., Construction of New Azo-group Containing Polycyclic Imidazole Derivatives: Computational Mechanistic, Structural, and Fluorescence Studies // ChemistrySelect, 5 -2020, p. 6224-6229.

20. Valadova G., Ahmadov O., Abdullayev Y., Bronsted acidic ionic liquid catalyzed conversion of monosaccharides to 5-hydroxymethylfurfural // IV International Scientific Conference of Young Researchers, Baku Engineering University, Baku/Azerbaijan, -2020, p. 391-392.

26. Sujayev A., Abdullayev Y., Theory for low-cost $[Et_2NH_2]HSO_4$ ionic liquid catalyzed CO_2 conversion to cyclic carbonates, cyclic carbamates, cyclic ureas, and cyclic carbonylsulfates // 5th Green and Sustainable Chemistry Conference, Dresden, Germany, -2020, p. P2.31.

29. Asadov Z.H., Ahmadova G.A., Rahimov R.A., Hashimzade S.-Z.F., Abdullayev Y., Ismailov E.H., Suleymanova S.A., Asadova N.Z., Zubkov F.I., Autschbach J., Aggregation and antimicrobial properties of gemini surfactants with mono- and di-(2-hydroxypropyl)ammonium head-groups: Effect of the spacer length and computational studies // Journal of Molecular Liquids, 302 -2020,

p. 112579.

30. Hasanov E.E., Rahimov R.A., Abdullayev Y., Asadov Z.H., Ahmadova G.A., Isayeva A.M., Ahmadbayova S.F., Zubkov F.I., Autschbach J., New class of cocogem surfactants based on hexamethylenediamine, propylene oxide, and long chain carboxylic acids: Theory and application // Journal of Industrial and Engineering Chemistry, 86 -2020, p. 123-135.

31. Hasanov E.E., Rahimov R.A., Abdullayev Y., Asadov Z.H., Ahmadova G.A., Isayeva A.M., Yolcuyeva U., Zubkov F.I., Autschbach J., Counterion-coupled gemini surfactants based on propoxylated hexamethylenediamine and fatty acids: Theory and application // Journal of Molecular Liquids, 318 -2020, p. 114050.

18. Abdullayev Y., TD-DFT studies of polycyclic imidazole derivative: 2-phenyl-1-(4-(phenyldiazenyl)phenyl)-1hphenanthro[9,10-]imidazole // Journal of Baku Engineering University - Chemistry and Biology, 4 -2020, p. 79-83

12. Abdullayev Y., Computational and experimental studies on [Et$_2$NH$_2$][HSO$_4$] ionic liquid catalyzed pyrazine and imidazole ring formation // PPOR, 22 -2021, p. 356-362.

14. Abdullayev Y., Computational insights of CF$_3$COOH catalyzed triazine formation reaction, Nakhchivan State University "Scientific Literatures". Series of Nature and Medicinal Sciences, 3 -2021, p. 174-176.

15. Sudjaev A., Abdullayev Y., Computer-based research of fine-organic synhesis methods for obtaining high-quality organic compounds // 1st International Congress on Natural Sciences (ICNAS-2021), Erzurum, Turkey, -2021

19. Abdullayev Y., Abbasov V., Nasirov F., Rzayeva N., Nasibova L., Autschbach J., Computational mechanistic studies of the carbon–carbon double bond difunctionalization via epoxidation and subsequent aminolysis in vegetable oils // International Journal of Quantum Chemistry, 121 -2021, p. e26609.

21. Abdullayev Y., Ahmadov O., Valadova G., Karimli A., Autschbach J., Unveiling the catalytic effects of Brønsted acidic ionic liquid on quantitative α-glucose conversion to 5-HMF: Experimental and computational studies // Renewable Energy, 171 -2021, p. 383-390.

22. Abdullayev Y., Standard curve method for determination of 5-hydroxymethylfurfural yield in a reaction mixture, Journal of Baku Engineering University - Chemistry and Biology, 5, -2021 p. 41-44.

27. Karimova N., Mammadaliyeva Z., Seyidova N., Abdullayev Y., Synthesis of cyclic urea from the reaction of n-(2-hydoxoethyl)ethylenediamine and carbon dioxide // V International Scientific Conference of Young Researchers, Baku Engineering University, -2021, p. 345.

23. Kazimi T., Abdullayev Y., Ionic Liquid catalyzed biomass conversion to 5-HMF // Conference on Enviromental Remediation, Granada (Spain), -2022, p. 14-15.

24. Abdullayev Y., Rzayev R., Autschbach J., Computational mechanistic studies on persulfate assisted p-phenylenediamine polymerization // Journal of Computational Chemistry, 43 -2022, p. 1313-1319.

25. Abdullayev Y., Javadova V., Valiyev I., Talybov A., Salmanov C., Autschbach J., Ionic Liquid-Mediated Urea Pyrolysis to Cyanuric Acid: Experimental Protocol and Mechanistic Insights // Industrial & Engineering Chemistry Research, 61 -2022, p. 15076-15084.

16. Israfilova Z., Taslimi P., Gülçin İ., Abdullayev Y., Farzaliyev V., Karaman M., Sujayev A., Alwasel S.H., Some Thiocyanate Containing Heterocyclic Compounds: Synthesis, Bioactivity and Molecular Docking Study // ChemistrySelect, 8 -2023, p. e202203653.

28. Abdullayev Y., Karimova N., Schenberg L.A., Ducati L.C., Autschbach J., Computational predictions on Brønsted acidic ionic liquid catalyzed carbon dioxide conversion to five-membered heterocyclic carbonyl derivatives // Physical Chemistry Chemical Physics, 25 -2023, p. 8624-8630.

The defense will be held on 5th December 2023 at 10:00 at the meeting of the Dissertation council ED 1.16 of Supreme Attestation Commission under the President of the Republic of Azerbaijan operating at Institute of Petroleum Processes, named after Yusif Mammadaliyev

Address: Khojali pr. 30, Postal code: Az 1025, Baku, Azerbaijan
Dissertation is accessible at the Institute of Petroleum Processes Library

Electronic version of the abstract is available on the official website of the Institute of Petroleum Processes

Abstract was sent to the required addresses on 2nd November 2023